

NASA TECHNICAL NOTE



NASA TN D-4362

C.1

NASA TN D-4362



LOAN COPY: RETU
AFWL (WLIL-2
KIRTLAND AFB, N MEX

**A QUASI-OMNIDIRECTIONAL SLOT ARRAY
ANTENNA FOR SPACECRAFT USE
AT MICROWAVE FREQUENCIES**

by W. F. Croswell, C. M. Knop, and D. M. Hatcher
Langley Research Center
Langley Station, Hampton, Va.



TECH LIBRARY KAFB, NM



0131368

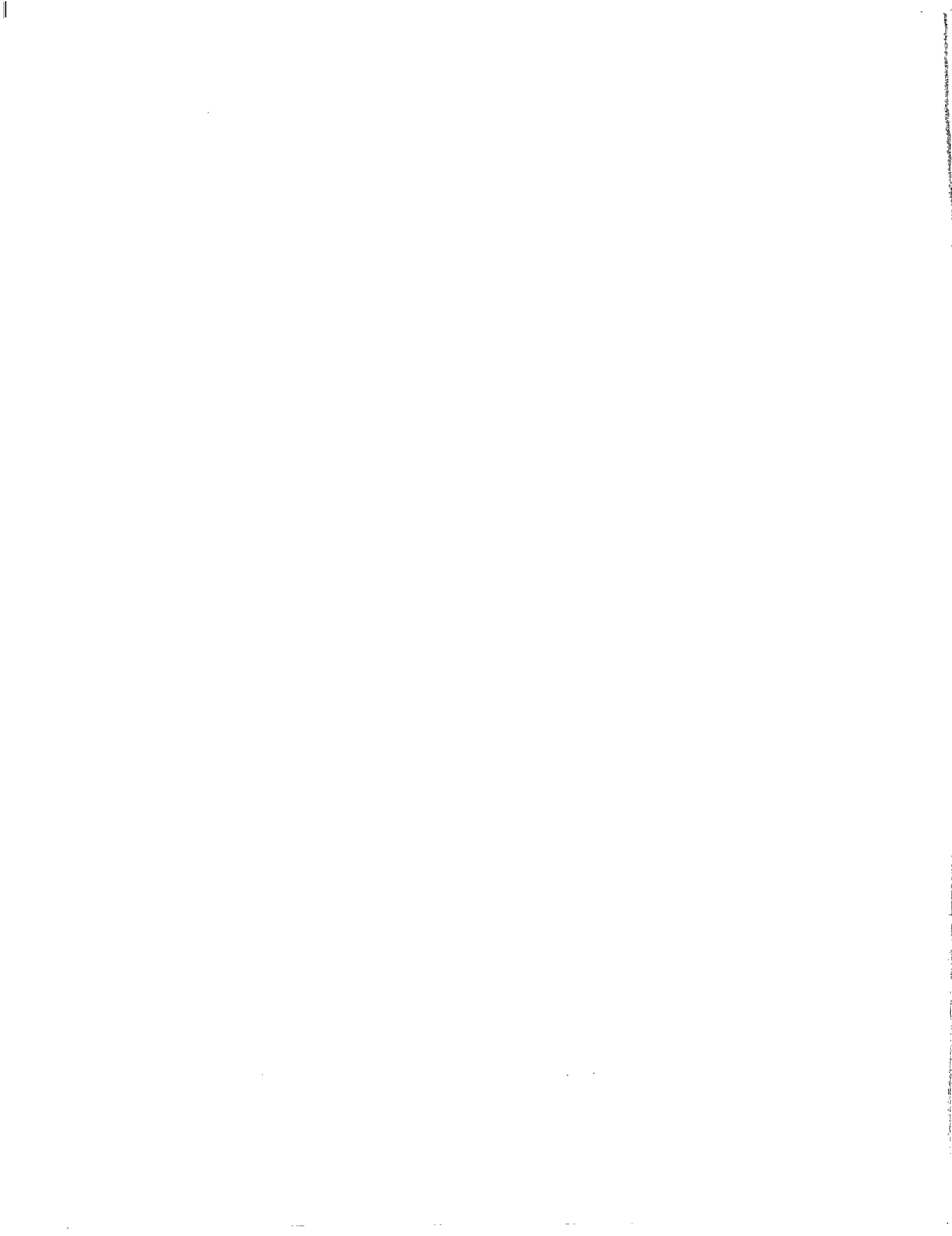
A QUASI-OMNIDIRECTIONAL SLOT ARRAY ANTENNA FOR
SPACECRAFT USE AT MICROWAVE FREQUENCIES

By W. F. Croswell, C. M. Knop, and D. M. Hatcher

Langley Research Center
Langley Station, Hampton, Va.

NATIONAL AERONAUTICS AND SPACE ADMINISTRATION

For sale by the Clearinghouse for Federal Scientific and Technical Information
Springfield, Virginia 22151 - CFSTI price \$3.00



CONTENTS

	Page
SUMMARY	1
INTRODUCTION	1
SYMBOLS	2
THEORY AND DESIGN	7
Determination of the Number of Slots	9
Ring Waveguide Design	9
Recess Design	10
Dielectric Cover Design	10
Calculations using theoretical idealized model	11
Radiation field computations for noncoated slot	13
Radiation field computations for coated slot	14
Slot Design	14
EXPERIMENTAL RESULTS	15
Radiation Patterns	15
Voltage Standing Wave Ratio Measurements and Gain	17
CONCLUDING REMARKS	17
APPENDIX A – THE THEORETICAL DEPENDENCE OF CIRCULAR ARRAY PATTERNS ON THE ELEMENT PATTERN SHAPE	19
APPENDIX B – A QUALITATIVE THEORY FOR PREDICTING RIPPLE EFFECTS IN THE CALCULATED AND MEASURED SINGLE SLOT PATTERNS	21
Plane Surface Waves	21
Theory	21
Calculations	24
Application	24
Pattern Ripples	24
Results	25
APPENDIX C – THE DESIGN OF SHUNT SLOTS IN THE BROAD WALL OF A WAVEGUIDE COVERED BY A DIELECTRIC LAYER	27
REFERENCES	31
FIGURES	33

A QUASI-OMNIDIRECTIONAL SLOT ARRAY ANTENNA FOR SPACECRAFT USE AT MICROWAVE FREQUENCIES

By W. F. Crosswell, C. M. Knop,* and D. M. Hatcher
Langley Research Center

SUMMARY

The theory, design, and development of a resonant array of circumferential shunt slots cut in the broad wall of a ring waveguide, which is recessed into a circular metallic cylinder and dielectric coated in the recessed region, are presented. This antenna is suitable for narrow bandwidth space-vehicle applications, since it is essentially flush mounted, provides nearly omnidirectional coverage in the plane perpendicular to the vehicle axis, and provides a broad pattern in the planes which are parallel to and pass through this axis.

The theory used for the design of the array is based upon the approximate synthesis method of Knudsen and Chu, in conjunction with the work of Wait for slots on dielectric-coated cylinders. The tolerance problems encountered in the development of the array and their solutions are discussed.

INTRODUCTION

The need to communicate through the plasma sheath formed around space vehicles during reentry into the earth's atmosphere has raised the operating frequency requirement of some of the telemetry systems used on the vehicles to those in the microwave range. Such operating frequencies will generally exceed the plasma frequency and make the plasma electrically transparent. The additional requirement of quasi-omnidirectional pattern coverage arises because of the nature of the tracking problem. Combined, these requirements lead to the necessity of providing a microwave flush-mounted antenna, mounted on surfaces with dimensions that are large in terms of wavelength. A typical case at X-band would be a cylindrical body approximately 18 to 24 inches in diameter and having a circumference of about 30 to 40 wavelengths.

In a recent paper (ref. 1), a solution to the problem of realizing such an antenna which produces vertical polarization (that is, polarization parallel to the vehicle axis) was suggested. The proposed antenna consisted of an array of uniformly excited

*Andrew Corporation, Chicago, Illinois.

circumferential slots flush with the cylinder, realized by cutting each slot in the broad wall of an air-filled rectangular waveguide in the form of a circle (that is, a ring waveguide) to form a resonant array of shunt slots. Each slot is successively spaced a half guide wavelength apart and alternately displaced from the center to realize a uniform phase and amplitude distribution.

Although a preliminary consideration of a similar array was made some time ago (ref. 2), only recently were the design and construction problems successfully solved. These solutions are described herein.

The array considered here is recessed into the cylindrical body and coated with dielectric for the following reasons:

- (1) To decrease the excitation of the mounting structure extremities, that is, to exercise control of the elevation (θ) plane pattern
- (2) To reduce the slot conductance
- (3) To seal the slots from their space environment
- (4) To insure the possibility of flush mounting

A photograph of the final version of the array developed is shown in figure 1 and its geometry is depicted in figure 2(a). The approximate theory and design of the recessed dielectric-coated array is based on an extension of reference 1, in conjunction with the work of Wait on slots on dielectric cylinders (ref. 3), as applied to dielectric-coated circumferential slots (ref. 4), and is given herein. The problems and their solutions, associated with the development and construction of the array, are also presented.

SYMBOLS

A	amplitude of assumed field
a	radius of ring waveguide
B	amplitude of assumed field
b	radius of dielectric cover
b_{\max}	maximum value of b
b_s	normalized slot susceptance
C	circumference of cylinder in wavelengths, $2\pi a/\lambda$

c velocity of light in a vacuum

D ripple in array pattern, dB

E fields of slot array

E_z assumed slot fields

E_ϕ electric field in ϕ -direction

$$E_{\theta_k} = V_0 \frac{e^{-j\beta_v r}}{\Gamma} f_k(\phi)$$

f frequency

$f_1(0)$ field pattern of one slot at $\phi = 0$

f_{c1} cutoff frequency in a parallel plate waveguide

$f_k(\phi)$ field pattern of any slot k

$$G_c = 1/R_c$$

$$G_{cv} = 1/R_{cv}$$

g conductance

g_s resonant slot conductance, coated case

g_v resonant slot conductance, uncoated case

H height of recess

$H_m^{(2)}(\)$ Hankel function, second kind

$$H_m^{(2)'}(\) = \frac{d}{dU} H_m^{(2)}(U)$$

H_0^+ amplitude of magnetic field, TE_{10} mode

$$H_0 = H_0^+(1 + \Gamma)$$

h phase constant

I constant current source, with cover

I_v constant current source, no cover

$J_m(\)$ Bessel function of first kind

$$J_m'(\) = \frac{d}{dU} J_m(U)$$

$J_z(\phi)$ surface current

$$j = \sqrt{-1}$$

K constant (eq. (B16))

k a particular slot

L length of mounting cylinder

l slot length

l_R length corresponding to average resonant frequency

m,n integer constants

$$N = \sqrt{\epsilon_r'}$$

P power coupled out by slot, under coating

P^+ incident power in TE_{10} mode

$P_1(\phi)$ power pattern of one slot

$|P(0)|$ normalized on-axis field value, $|f_1(0)|$

P_v	power coupled out by slot, no coating
q	image radiator source strength
R_c	slot radiation resistance, coated case
R_{cv}	slot radiation resistance, uncoated case
r	coordinate direction $\sqrt{x^2 + y^2 + z^2}$
\bar{r}	radius of ring waveguide to waveguide center line
r_o	radius of mounting cylinder
S	number of sources in circular array
$T = b - a$	
t	thickness of ungrounded sheet
$TE()$	a particular transverse electric surface wave mode
TE_{10}	mode description, dominant mode in rectangular waveguide
$TM()$	a particular transverse magnetic surface wave mode
U	dummy variable
$U_m = J_m(NC) H_m^{(2)}(NCW) - J_m'(NCW) H_m^{(2)}(NC)$	
$V_m = J_m(NC) H_m^{(2)}(NCW) - J_m(NCW) H_m^{(2)}(NC)$	
V_o	slot excitation voltage
$W = b/a$	
ΔW	increment of W



- w slot width
- x,y,z, ρ coordinate directions
- x',y',z' coordinates for plane sheet model
- x₀ waveguide height
- x_s slot displacement from center line
- y_s resonant slot admittance, coated case
- y₀ waveguide width
- α attenuation constant
- $\beta = \frac{2\pi}{\lambda_v}$
- β_v wave number in a vacuum, $2\pi/\lambda_v$
- Γ reflection coefficient; conjugate of Γ^*
- $\delta_0^m = \begin{cases} 1 & (m = 0) \\ 2 & (m \neq 0) \end{cases}$
- $\epsilon = \epsilon_r' \epsilon_v$
- ϵ_1, ϵ_2 permittivity in mediums 1 and 2, respectively
- ϵ_r' relative dielectric constant
- ϵ_v permittivity of vacuum
- η intrinsic impedance of medium ϵ_r'
- η_v intrinsic impedance of vacuum
- θ polar coordinate angle
- θ_f phase of slot field
- λ wavelength in a dielectric medium
- λ_c cutoff wavelength in waveguide
- λ_{c1} cutoff wavelength in parallel plate waveguide

λ_g	guide wavelength
λ_R	wavelength corresponding to f_R
λ_v	wavelength in vacuum
μ	permeability of medium
μ_1, μ_2	permeability in mediums 1 and 2, respectively
μ_r^*	relative permeability
μ_v	permeability of vacuum
ρ_0	a particular radius
τ	thickness of waveguide wall
Φ	array pattern, synthesis method
Φ_{\max}	maximum value, array pattern
Φ_{\min}	minimum value, array pattern
ϕ	azimuthal angle
$\Delta\phi$	increment of ϕ
ϕ_k	a particular angle in azimuthal direction
ϕ_0	angular slot width, l/a
$\omega = 2\pi f$	

An asterisk on a symbol denotes a conjugate.

THEORY AND DESIGN

To design the subject antenna by using an exact formulation would involve solving at least a five-region boundary-value problem as depicted in figure 2(a). However, because of the large number of parameters and the likely complexity of the resulting transcendental equations involved, it was decided to adopt an engineering approach in the design of this antenna.

The basic recognition in this design was that the required recessing and dielectric covering would act as perturbation effects upon the performance of a flush-mounted array

on an infinitely long noncoated cylinder designed to produce the desired omnidirectional equatorial plane pattern. Thus, if the array were initially designed on a flush-mounted noncoated cylinder of the specified size and the pattern perturbations caused by recessing and coating could be determined, the latter factors could be chosen to produce the smallest perturbations. As such, the first step in the antenna design was to design the array (ref. 1) as if it were flush mounted on an infinitely long noncoated cylinder; secondly, to choose the ring waveguide dimensions appropriately; and then to recess the array (by increasing the radius of the housing cylinder in which the designed array is inserted) the proper amount to bring the elevation plane pattern to its desired form. The recessing controls the image sources established at the axial extremities of the cylinder because of the interruption of axial surface current flow. (See ref. 5.) With the recess properly chosen (this choice was made empirically), the change in array equatorial plane patterns due to a dielectric cover of a specified dielectric constant ϵ_r' and with thickness as a parameter was then approximately determined by using the work of Wait (ref. 3) and Knop (ref. 4) in conjunction with an approximate synthesis method. This step reveals the range of cover thicknesses which can be used with little influence on the equatorial plane patterns. A reasonable thickness in this range was then chosen, which was also observed by experiments to have little effect on the elevation plane pattern. The dielectric-cover parameters being chosen, the slot dimensions and slot displacement were then determined by insisting that the antenna be reasonably matched to the feed waveguide at the design frequency and throughout the bandwidth specified. The choice of slot dimensions was based upon the work on slot conductances on dielectric-coated ground planes. (See ref. 6.) Thus, the design of the subject antenna can be divided into the following five major steps:

- (1) Determination of the number of slots S for a specified departure from omnidirectionality D
- (2) Ring waveguide design (excluding slot design)
- (3) Recess design
- (4) Dielectric cover design
- (5) Slot design.

The explicit parameters as determined by each step are given in the following table. The optimum design will require several iterations of these steps with either r_0 or a fixed.

Step	Parameters
1	a, S
2	Waveguide size
3	r_0, H, a
4	ϵ_r', b
5	l, w, x_s

Determination of the Number of Slots

For a specified cylinder radius a and a specified operating frequency f , the determination of the number of slots S in an infinite uncoated cylinder required to produce an equatorial plane pattern having a maximum specified deviation from omnidirectionality D was accomplished exactly as described in reference 1. Reference 1 is based on the work of Knudsen (ref. 7) and Chu (ref. 8). The specified diameter of the cylinder $2a$ was $16\frac{5}{32}$ inches (41.05 cm) and the specified frequency f was 9.21 GHz and corresponds to $C = 39.5$. The equatorial plane pattern was to be omnidirectional within ± 0.50 dB, that is, $D = 1$ dB. These requirements were dictated by a likely application. By using figure 2 of reference 1, the number of slots required is determined as being greater than 46 for $C = 39.5$.

A choice of 54 slots was made because the departure from the specified omnidirectionality was less for this number of slots over a wider bandwidth (that is, for a larger variation of C about 39.5; see fig. 2 of ref. 1) than that obtained by a smaller number of slots. Additionally, this number can be made to satisfy the requirement of a half guide wavelength (for RG-52/U waveguide) between slots as will be discussed subsequently.

With such a large number of slots, calculations (ref. 1) reveal that the array pattern is very insensitive to the element pattern (that is, the pattern from an individual slot), and thus allows a wide latitude in the assumption of slot voltage distribution without affecting the array pattern.

Ring Waveguide Design

The waveguide size must be chosen so that the arc spacing between the center of two successive slots, as measured along the circular line in the middle of the guide, is a half guide wavelength.

It is assumed that the propagation in the curved guide is such that the phase velocity, and therefore λ_g , in the center of this guide is not altered from that of a straight guide of the same cross section. This assumption is reasonable for the large radius

used. Reference to figure 3, which depicts the ring waveguide geometry, shows that

$$\bar{r} = a - \frac{\tau + y_0}{2} \quad \bar{r} = a - \tau - \frac{y_0}{2}$$

Choosing the RG-52 U waveguide, $\tau = 0.050$ inch (0.127 cm), $y_0 = 0.400$ inch (1.016 cm), and $\lambda_c = 2x_0 = 1.800$ inches (4.572 cm), $\lambda_v = 1.280$ inches (3.25 cm) ($f = 9.21$ GHz), and $2a = 16\frac{5}{32}$ inches (41.05 cm), dictates that $S = 54$, which has already been shown to be compatible with the specified omnidirectionality requirements.

Recess Design

The housing cylinder radius r_0 was chosen so that with no dielectric coating, the distance from the source point (that is, the surface $\rho = a$) to the edge of the cylinder (that is, $\frac{L}{2} + (r_0 - a)$) is an integral number of "effective" half wavelengths. This condition causes the strength q of the equivalent image radiators at the edges of the cylinder to be a minimum and, hence, the elevation plane pattern which is approximately $1 + 2q \cos\left(\pi \frac{L}{\lambda_v} \sin \theta\right)$ to have less severe amplitude variations (ref. 5).

Since the "effective" wavelength from the source point to the edge of the cylinder is not really known beforehand, this recess depth will, in general, have to be empirically determined. For the antenna considered ($L = 12$ inches (30.48 cm), $2a = 16\frac{5}{32}$ inches (41.05 cm)), it was found that a choice of $r_0 - a = 0.703$ inch (1.79 cm) (that is, $2r_0 = 17\frac{9}{16}$ inches (44.6 cm)) resulted in the most satisfactory elevation plane patterns.

The recess height H was chosen sufficiently small so that the first higher order mode in the radial guide (which is approximately the TM mode between two parallel planes for this large cylinder and short length of radial walls) cannot propagate in the air-filled recess. The cutoff wavelength λ_{c1} for this mode is $\lambda_{c1} = 2H$; therefore, a choice of $H = 0.5$ inch (1.27 cm) gives $\lambda_{c1} = 1.00$ inch (2.54 cm) and a corresponding cutoff frequency of $f_{c1} = 11.8$ GHz, which is well above the operating frequency of 9.21 GHz, so that this mode and all higher modes cannot propagate. The choice of $H = 0.5$ inch (1.27 cm) was also found to provide satisfactory elevation plane patterns, whereas choice of a larger H broke up these patterns and choice of a smaller H causes interference with the finite width slots.

Dielectric Cover Design

With the recess depth determined, it is next necessary to choose an appropriate dielectric cover. The material chosen was, for convenience of machining, plexiglass, $\epsilon_r' = 2.54$; the thickness was determined by the criteria that the specified omnidirectionality of the equatorial plane radiation patterns was to be affected as little as possible and that the elevation plane pattern was to be essentially preserved.

Calculations using theoretical idealized model.- To obtain the equatorial-plane radiation-pattern dependence on dielectric-coating thickness for the specified ϵ_r' , the model shown in figure 2(b) was used. This model neglects the effect of the recessing and the effect of finite cylinder length. The latter, as far as the equatorial plane radiation pattern is concerned, is justified on the basis of previous analytical work on both coated (ref. 4) and noncoated cylinders (ref. 9). This work shows that, for a sufficiently long cylinder, the equatorial plane pattern is approximately independent of cylinder length.

As was discussed in step 3, the desirable effect of recessing is to produce diffraction at the edges of the recess, which can be used to control the elevation plane pattern. Additionally, however, the recess can act as a channel waveguide and, hence, can cause more energy to propagate around the cylinder and cause more radiation in the back direction, as compared with the nonrecessed case. This criticism of the model of figure 2(b) is probably the most severe. However, even though the patterns of a single recessed slot may differ appreciably in the back direction, as compared with a nonrecessed one (as will be shown later), the fact that there are such a large number of elements causes little change in the array pattern. Hence, the model of figure 2(b) was still adopted. Additionally, the model of figure 2(b) is taken with all slots centered at the plane $z = 0$; the consequence of this assumption is discussed later.

In the model array of figure 2(b), the electric field over each slot is assumed to be of equal magnitude and phase; therefore, any arbitrary slot (say, the k th slot) the center of which is at the angle ϕ_k , is assumed to be excited with an E_z field of the form

$$\left. \begin{aligned} E_z(a, \phi, 0) &= 0 && \text{(Off slot)} \\ E_z(a, \phi, 0) &= \sin \left\{ C \left[\frac{\phi_0}{2} + (\phi - \phi_k) \right] \right\} && \left(\phi_k - \frac{\phi_0}{2} \leq \phi \leq \phi_k; \text{ On slot} \right) \\ E_z(a, \phi, 0) &= \sin \left\{ C \left[\frac{\phi_0}{2} - (\phi - \phi_k) \right] \right\} && \left(\phi_k \leq \phi \leq \phi_k + \frac{\phi_0}{2}; \text{ On slot} \right) \end{aligned} \right\} \quad (1)$$

where

ϕ_0 angular slot width, l/a

l length of slot

C circumference of cylinder in free-space wavelengths, $\frac{2\pi a}{\lambda_v}$

λ_v free-space operating wavelength

Additionally, the E_ϕ field on the slot, since it is very narrow, is taken as zero; that is,

$$E_\phi(a, \phi, z) = 0 \quad (2)$$

The distribution of equation (1) is reasonable, since it is similar to that of a standing wave of current on a thin wire excited at its center. With a knowledge of the tangential electric fields over the k th slot, the radiation fields produced by this slot can be found by using the general method of Wait (ref. 3). For the specific problem of a circumferential slot excited according to equations (1) and (2) on a coated or noncoated cylinder, the equatorial plane radiation fields produced are (eq. (55) of ref. 4, with ϕ replaced by $(\phi - \phi_k)$).

$$E_{\theta k}(r, \frac{\pi}{2}, \phi) = \sqrt{\frac{\mu_v}{\epsilon_v}} H_\phi(r, \frac{\pi}{2}, \phi) = V_0 \frac{e^{-j\beta_v r}}{r} f_k(\phi) \quad (3)$$

where

$$f_k(\phi) = -\frac{4}{\pi^3} \left(\frac{1}{W}\right) \sum_{m=0}^{\infty} \frac{j^m \left[\cos\left(\frac{m\phi_0}{2}\right) - \cos\left(C \frac{\phi_0}{2}\right) \right] \cos m(\phi - \phi_k)}{(C^2 - m^2)(1 + \delta_0^m) \left[NH_m^{(2)}(CW) U_m - H_m^{(2)'}(CW) V_m \right]} \quad (4)$$

where

$$\delta_0^m = \begin{cases} 1 & (m = 0) \\ 0 & (m \neq 0) \end{cases}$$

and

$$U_m = J_m(NC) H_m^{(2)'}(NCW) - J_m'(NCW) H_m^{(2)}(NC) \quad (5)$$

$$V_m = J_m(NC) H_m^{(2)}(NCW) - J_m(NCW) H_m^{(2)}(NC) \quad (6)$$

with

$$N = \sqrt{\epsilon_r'}$$

$$W = b/a$$

For the special case of no coating ($N = \epsilon_r' = 1$ and/or $W = 1$), $f_k(\phi)$ reduces to

$$f_k(\phi) = -j \frac{2C}{\pi^2} \sum_{m=0}^{\infty} \frac{j^m \left(\cos \frac{m\phi_0}{2} - \cos \frac{C\phi_0}{2} \right) \cos m(\phi - \phi_k)}{(C^2 - m^2)(1 + \delta_0^m) H_m^{(2)}(C)} \quad (7)$$

which is the correct result. (See ref. 4.) For any array of S circumferential slots, the total field produced is the sum of the field produced by each of the k th slots; that is,

$$E\left(r, \frac{\pi}{2}, \phi\right) = \sum_{k=1}^S E_{\theta_k} = V_0 \frac{e^{-j\beta_v r}}{r} \sum_{k=1}^S f_k(\phi) \quad (8)$$

This superposition neglects the effect of mutual coupling between slots, which may tend to change the slot distribution from that assumed; however, for a linear shunt-slotted array, it has been shown (ref. 10) that such coupling is trivial, since very little of the surface current established by one slot intercepts another slot. Since this condition will also hold here, this assumption is taken as equally valid.

The power radiation pattern $P_1(\phi)$ is then given in decibels by

$$P_1(\phi) = 20 \log_{10} \left| \frac{E_{\theta}\left(r, \frac{\pi}{2}, 0\right)}{E_{\theta}\left(r, \frac{\pi}{2}, \phi\right)} \right| \quad (9)$$

Radiation field computations for noncoated slot.- The equatorial plane radiation field for a noncoated single slot, centered at the origin (that is, $\phi_1 = 0$) for a cylinder of $2a = 16\frac{5}{32}$ inches (41.05 cm) and a slot length of $l = 0.500$ inch (1.27 cm) operating at a frequency of 9.210 GHz was computed by using equation (7). A plot of the normalized field quantity

$$\left| \frac{E_{\theta}\left(r, \frac{\pi}{2}, \phi\right)}{E_{\theta}\left(r, \frac{\pi}{2}, 0\right)} \right| = \left| \frac{f(\phi)}{f(0)} \right|$$

is shown in figure 4(a). A plot of the phase θ_f where $f(\phi) = |f(\phi)|e^{j\theta_f}$ is plotted in figure 4(b) and a power radiation pattern $P_1(\phi)$ is shown in figure 5. It was found that 80 terms in the summation of equation (7) give four significant figure accuracy in both the magnitude and phase of $f(\phi)$. From equations (8) and (9), the pattern of an uncoated 54 slot array was then computed. Inspection of equation (8) for this case reveals that the field of the array is periodic in ϕ , periodicity being $\frac{360}{54}$ or $6\frac{2}{3}^\circ$. Computation of the radiation pattern $P_1(\phi)$ in increments $\Delta\phi$ of 1° revealed that the pattern was omnidirectional within ± 0.10 dB and hence the pattern is not drawn here. It is seen that this

deviation in omnidirectionality is in good agreement with the approximate synthesis method used. (See appendix A.)

Radiation field computations for coated slot.- Computations of the radiation field were performed for the single slot case by using equation (4) for a coating of $\epsilon_r' = 2.54$ and of variable thickness on this cylinder and with the same slot excitation as used for the no coating case.

The resultant radiation power patterns $P_1(\phi)$ as a function of coating thickness T are shown in figures 6(a) to 6(c). Increments in thickness of 0.0323 inch (0.82 cm) were used corresponding to $\Delta W = 0.004$. The case of the cylinder being flush with the outside cylinder wall, that is, $b = r_0$ where $2r_0 = 17\frac{9}{16}$ inches (44.6 cm) was also computed.

An inspection of figures 6(a) to 6(c) for the single-slot case reveals that the patterns broaden with increasing W and are not oscillatory for $1 \leq W \leq 1.032$. A further increase in thickness causes ripples and oscillations to occur in the rear direction. For $1.04 \leq W \leq 1.05$, significant lobes of radiation occur in the rear direction.

In particular, it is noted from figure 6(b) for the case of a 0.3555-inch-coating thickness (that is, $W = 1.044$) that the pattern has many nearly equal lobes all about the cylinder. It is noted from these patterns that the element pattern is very sensitive to thickness for a fixed frequency and for a fixed dielectric constant.

A further increase in W causes the patterns again to resemble that of the non-coated case ($1.056 \leq W \leq 1.096$) but becoming much broader for the higher W values ($1.084 \leq W \leq 1.096$). Thus, maximum ripple effects occur in the range of $1.04 \leq W \leq 1.052$ and correspond to a thickness range of $0.32 \text{ inch} \leq T \leq 0.42 \text{ inch}$ ($0.81 \text{ cm} \leq T \leq 1.07 \text{ cm}$) or $0.4 \leq \frac{T}{\lambda} \leq 0.5$. A detailed analysis of the ripple effects is given in appendix B.

All array patterns computed by using equation (9) for the values of W of figures 6(a) to 6(c) (including those for which the element pattern has many almost equal lobes about the cylinder) were within ± 0.5 dB of being omnidirectional and, hence, are not plotted here. This theoretical finding is also in agreement with that based on the approximate synthesis method, which also predicts that unless the element pattern is almost perfectly omnidirectional, the array pattern will be omnidirectional, as shown in appendix A. It is noted that 54 cycles occur in each pattern. The value $|P(0)|$ on each figure is the normalized-on-axis ($\phi = 0^\circ$) electric field value; that is, $|P(0)| = |f_1(0)|$ where $f_1(0)$ is given by equation (5) with $\phi_1 = 0$.

Slot Design

The resonant array is depicted in figure 7, along with its equivalent circuit (ref. 11). The individual normalized slot admittance $y_s = g_s + jb_s$, is to be made so that the resonant slot conductance g_s is a maximum for a given slot displacement x_s . (See ref. 10.)

For the specified design frequency f and dielectric constant ϵ_r' , and a conventional slot width w of 0.0625 inch (0.159 cm), the slot length l required for resonance is obtained from the generalized empirical curve (ref. 6) of figure 8. This curve shows the slot length required for resonance of $1 \leq \epsilon_r' \leq 4$ and for any coating thickness T of $T \geq 0.2\lambda$, where λ is $\lambda_v/\sqrt{\epsilon_r'}$. The curve is empirical and is believed to give results for resonant length accurate to within 5 percent. It is seen that the slot length required for resonance is lowered by use of a sufficiently thick dielectric cover. For $\epsilon_r' = 2.54$ and $f = 9.21$ ($\lambda_v = 1.28$ inches (3.25 cm)) this curve gives $l = 0.494$ inch (1.25 cm). It is noted that this slot length differs only slightly from that used in the pattern computations of figure 6, namely, $l = 0.500$ inch (1.27 cm).

The remaining slot dimension to be determined is the displacement x_s . Reference to figure 7 shows that the required resonant slot conductance for a match to exist at the input to each half of the array (that is, $27g_s = 1$) is

$$g_s|_{\text{Required}} = \frac{1}{27} = 0.037 \quad (10)$$

At resonance, the slot conductance is given by

$$g_s = K \sin^2\left(\pi \frac{x_s}{x_0}\right) \quad (11)$$

where K is a modified form of Stevenson's constant (ref. 12) as shown in appendix C.

It is noted that, for a given slot displacement, the dielectric coating decreases the slot conductance as compared with the noncoated case (that is, K decreases with increasing ϵ_r'). This decrease enables the choice of a higher value of x_s for a specified g_s ; hence, one can realize longer arrays with a coating, as compared with arrays without a coating.

For the case of $\epsilon_r' = 2.54$, $f = 9.21$ GHz, and for any coating thickness $T \geq 0.2\lambda \approx 0.16$ inch (0.41 cm), it follows from appendix C that $K = 0.535$ and, hence, from equations (11) and (12) for a match $x_s = 0.103$ inch (0.26cm).

EXPERIMENTAL RESULTS

Radiation Patterns

Initial equatorial plane patterns of a constructed recessed array with no dielectric coating were found to be within ± 3 or more decibels of omnidirectionality. It was found that these poor results were primarily due to the asymmetrical location of the short-circuiting plate at the middle of the array, that is, at the point diametrically opposite



from the feed point. The location of this plate is very critical, since, unless it is exactly at the center of the array, the impedance it presents to the last slot of each half of the array will differ, and results in progressively unequal power excitation of each half of the array. It was found that the best way to realize a symmetrical short was to connect that half of the array opposite the feed point to another H-plane bend and to terminate it with a movable short, as shown in figure 7. In this way the equatorial plane patterns measured were made omnidirectional within ± 1 dB at the design frequency of 9.21 GHz as shown in figure 9(a). This deviation is acceptable for the applications discussed, even though it is in excess of that specified in the design.

The corresponding measured elevation plane array pattern (ϕ fixed, θ variable) for the no coating case, is shown in figure 9(a) for the case of $\phi = 0$ (which is a representative pattern for all other values of ϕ) and is also seen to be that desired.

Coating thicknesses corresponding approximately to some of those for which the computations were made (fig. 6) were then placed on the array, and for each thickness the equatorial plane and elevation plane patterns were measured. In addition, a ring waveguide containing a single slot was also constructed and patterns also were measured by utilizing these coatings. The element and array patterns are shown in figure 9.

A comparison of figure 9 with the corresponding patterns of figure 6 shows that the effect of the coating is essentially as predicted by figure 6, despite the fact that the effect of recessing was neglected in the theory. In particular, from figures 9(b) and 9(c), it is seen that the element pattern has many almost equal lobes all about the cylinder for a coating thickness in the range of 0.30 (0.76 cm) to 0.35 inch (0.89 cm). A serious deviation from omnidirectionality of the array pattern can possibly be expected, precisely as observed for the thickness of 0.35 inch (0.89 cm) (fig. 9(c)). This random-error type of pattern was due to the tolerance errors in dielectric thickness or dielectric constant. When the contributions from all 54 slots are significant, the random errors become important.

It should be mentioned that the "critical" coating thickness is intimately related to the surface waves which can exist in the dielectric coating. A brief discussion of this problem is given in appendix B.

From the experimental curves of figure 9, it is seen that satisfactory antenna patterns result for practically any choice of dielectric thickness (although some thicknesses introduce slightly less ripple than others) in the range of 0.20 (0.51 cm) to 0.71 inch (1.80 cm), with the exception of the critical thickness of near 0.35 inch (0.89 cm).

Similar conclusions also hold for the frequency band between 9.15 to 9.25 GHz, as revealed by similar measurements made at these frequency extremes.

It is also noted from figure 9 that 27 ripples, and not 54 as predicted, occur in the equatorial plane patterns. It is presumed here that this result is due to the fact that for the model used to predict the patterns, the effect of slot asymmetry was neglected. A similar situation was observed for a linear array of recessed slot elements (ref. 13).

Voltage Standing Wave Ratio Measurements and Gain

Typical voltage standing wave ratio (VSWR) characteristics of the array are shown in figure 10 for a coating thickness of $T = 0, 0.20$ (0.51 cm), 0.25 (0.63), and 0.30 inch (0.76 cm). For each thickness the antenna was matched at the design frequency by slightly adjusting the terminal short circuit position at the point opposite from the feed point. The slight adjustment to accomplish this match did not affect the radiation patterns. Although the procedure of slot design is adequate for an array without a recess, the effect of the recess upon the slot impedance is such that some additional final adjustment is necessary to obtain an acceptable value of input VSWR. The adjustment of the terminating short circuit merely changes the terminal impedance seen by each of the 27 slot arrays in such a way that a match over a narrow range of frequencies is insured. The antenna can be matched throughout the pattern bandwidth of 9.15 GHz to 9.25 GHz for any thickness of coating considered except 0.31 inch (0.76 cm). The VSWR curves for thicknesses greater than 0.3 inch are similar to that for 0.3 inch (0.76 cm) and therefore were not included. The bandwidth of the VSWR curves, although smaller than the bandwidth ($\pm 50/S$) percent of resonant arrays (ref. 10), is adequate for space vehicle applications where only information bandwidths of ± 5 MHz are required.

The measured gain is indicated in figure 9. For the case of $T \geq 0$ the gain in the ϕ plane averages about -2 to -3dB below isotropic level.

CONCLUDING REMARKS

It has been shown how a microwave waveguide resonant array of circumferential slots in a dielectric-filled recessed region of a metal circular cylinder whose dimensions are large in terms of wave lengths can be designed and constructed to provide essentially omnidirectional coverage in a plane perpendicular to the axis of the cylinder and to provide a broad main beam in any plane parallel to and passing through this axis.

The basic finding in this work is that for a specified frequency, cylinder radius, and coating dielectric constant, there exists a coating thickness, here defined as the "critical" coating thickness, which causes the pattern from a single slot to have many almost equal lobes all about the cylinder and that for this thickness (and thicknesses close to it), the associated array pattern can deteriorate very much from omnidirectionality in a random fashion because of tolerance errors. Any other thickness of dielectric

coating not near or equal to this critical thickness has little effect on the array omnidirectionality. Furthermore, this critical thickness can be predicted.

By taking into account the reduction of slot conductance caused by the dielectric coating in the manner discussed, an estimate of how the array can be matched over a bandwidth approximately that typifying resonant arrays can be obtained. This estimate is made by using a greater slot displacement and a shorter slot length for each slot, as compared with the noncoated case. However, the effect of recessing will modify this estimate and cause some reduction of bandwidth because of the addition of tuning. Hence, further empirical study of the effect of the recess design upon individual slot impedance characteristics will be required for particular array designs. Such an impedance study can improve the VSWR characteristics observed in this paper.

The addition of a dielectric material in the recess can affect the elevation pattern, that is, allow higher order modes in the parallel plate region. However, from a careful observation of measured patterns, one can comment that this effect is noticeable but not serious and hence the array can be flush-mounted.

Finally, it should be noted that during the process of making impedance and pattern measurements with the various thickness rings, it was necessary to disassemble the recess plates and ground plane numerous times. It was found that this operation had little effect upon repeatability of pattern and impedance measurements.

Hence, by using the design procedure described, a successful X-band array was constructed. The same design procedure can also be used for antennas throughout the microwave frequency range.

Langley Research Center,
National Aeronautics and Space Administration,
Langley Station, Hampton, Va., June 19, 1967,
125-22-02-02-23.

APPENDIX A

THE THEORETICAL DEPENDENCE OF CIRCULAR ARRAY PATTERNS ON THE ELEMENT PATTERN SHAPE

Consider the subject array of S identical elements fed in phase and with equal amplitude. The equatorial plane pattern of the array $\Phi(\phi)$, can be approximately expressed as (ref. 8).

$$(\Phi) \approx S \sum_{n=0}^N A_n (-j)^n \frac{d^n}{dC^n} \left[J_0(C) + 2j^S J_S(C) \cos S\phi \right] \quad (A1)$$

where A_n is the coefficient in the expansion of the element pattern

$$f(\phi) = \sum_{n=0}^N A_n \cos^n \phi \quad (A2)$$

The amount of ripple D in the array pattern, that is, the deviation from a true circle, is defined in decibels by

$$D = 20 \log_{10} \frac{|\Phi_{\max}|}{|\Phi_{\min}|} \quad (A3)$$

In order to obtain an idea of how sensitive the array pattern is upon the degree of omnidirectionality of the element pattern $F(\phi)$, expression (A2) was truncated to two terms as

$$F(\phi) = A_0 + A_1 \cos \phi \quad (A4)$$

Such an expression represents the pattern of many typical small slot antennas that might be used in circular arrays. Consider the case of $A_0 = 1$, $A_1 = 0$, that is, the omnidirectional element pattern case. The array pattern can then be expressed as¹

$$\Phi(\phi) \approx S \left[J_0(C) + 2j J_S(C) \cos \phi \right] \quad (A5)$$

¹It is interesting to note that the term $J_0(C)$ in equation (A5) represents the radiation pattern (which is omnidirectional) of a uniform continuous source distribution over the cylinder surface; the fact that the actual source distribution is composed of a discrete number of radiators is manifested by the additional term in equation (A5) which introduces ripples and which vanishes in the limit of a continuous distribution (that is, for $S \rightarrow \infty$, $J_S(C) \rightarrow 0$).

APPENDIX A

For this case, the array pattern has infinite ripple, regardless of the number of elements if $J_0(C) = 0$. To determine how close to a circle the element pattern must be to obtain very large ripple in the array pattern, computations were made by utilizing equation (A1) for $A_0 = 1$ and $A_1 = 0.001, 0.005, 0.01, 0.025, 0.0625, 0.125, 0.250,$ and 0.50 in order. A sketch of these element patterns is given in figure 11 and the ripple D is plotted in figure 12 as a function of C for $S = 54$. The data plotted were restricted to $39.9 \leq C \leq 40.20$ for clarity. For $39 \leq C \leq 39.9$ and $40.2 \leq C \leq 41$, all curves have $D < 0.03$ dB. It should be noted that the adjacent zeroes of $J_0(C)$ occur at $C = 36.92$ and 43.20 . It is clear from an inspection of figure 12 that the element pattern must be omnidirectional within $A_1 \leq 0.001$ (that is, within approximately 0.002 dB) to obtain an array ripple D of 4 dB or greater.

This theoretical finding predicts that the element pattern must be almost perfectly omnidirectional for any significant ripple to occur in the array pattern.

APPENDIX B

A QUALITATIVE THEORY FOR PREDICTING RIPPLE EFFECTS IN THE CALCULATED AND MEASURED SINGLE SLOT PATTERNS

Ripples are observed in both the theoretical and experimental patterns of dielectric-coated slots on a cylinder. (See figs. 6 and 9.) Such ripples appear to be strongly dependent upon the coating thickness T ; indeed, it was noted earlier that there is a "critical thickness" which must be avoided if predictable and desirable array patterns are to be achieved. Hence, even a qualitative determination of such a "critical thickness" will be of value to the designer.

Consider the case of a half-wave circumferential slot on a cylinder that has a circumference C that is large in terms of a wavelength, that is, $C = 39.5$. The pattern in the equatorial plane of the slot in this case is very similar to that of a slot on an infinite flat conducting groundplane (ref. 14) for the instance when neither slot is dielectric coated. Large amounts of power were observed to be opposite from the slot on the dielectric-coated cylinder $\epsilon_r' = 2.54$, for certain dielectric thicknesses. (See figs. 6 and 9.) Such large amounts of power do not exist in the rearward region of the pattern ($\phi \approx 180^\circ$) for the uncoated case. Hence, the rearward energy is due to trapping, guiding, and reradiation of slot energy by the dielectric layer. Because of the noted similarity of the slot patterns of flat groundplanes and large cylinders, it was deduced that a study of surface-wave modes in plane grounded dielectric sheets might give an insight into the trapping and guiding effects. Reradiation of the surface wave energy is due to the curved surface analogous to antenna designs (refs. 10 and 15) and is discussed in general by Barlow and Brown (ref. 16).

Plane Surface Waves

Theory.- Consider the diagram shown in figure 13. Here is depicted a dielectric sheet which extends to infinity in both the x' - and z' -directions. It is considered that the fields are two-dimensional and have no variation in the y' -direction. The trapped waves are considered to be traveling waves in the z' -direction. The fields can be found in a set of TE or TM modes relative to either the x' - or z' -direction. In this case the z' -direction is chosen. The regions I and III can be chosen to be arbitrary linear isotropic regions with any ϵ, μ property; in this case, air is chosen so that $\mu = \mu_v$ and $\epsilon_1 = \epsilon_v$. The region II is also arbitrary and is chosen to be $\mu_2 = \mu_v$, $\epsilon_2 = \epsilon_r' \epsilon_v$. From these assumptions, the following fields are obtained (see ref. 17, pp. 43-83):

APPENDIX B

For the TE_m modes,

$$Ey' = Be^{-\alpha x'} e^{-jhz'} \quad (\text{Region I}) \quad (\text{B1})$$

$$Ey' = A \cos\left(\frac{kx' - m\pi}{2}\right) e^{-jhz'} \quad (\text{Region II}) \quad (\text{B2})$$

$$Ey' = (-1)^m Be^{\alpha x'} e^{-jhz'} \quad (\text{Region III}) \quad (\text{B3})$$

Similarly, for the TM_m modes,

$$Hy' = Be^{-\alpha x'} e^{-jhz'} \quad (\text{Region I}) \quad (\text{B4})$$

$$Hy' = A \cos\left(\frac{kx' - m\pi}{2}\right) e^{-jhz'} \quad (\text{Region II}) \quad (\text{B5})$$

$$Hy' = (-1)^m Be^{\alpha x'} e^{-jhz'} \quad (\text{Region III}) \quad (\text{B6})$$

The distinguishing property of surface waves is the exponential decay of the fields in the x' -direction away from the sheet. Since the value of α will decrease for decreasing t , ω , or $\mu_2\epsilon_2$, the value of α will become zero if t , ω , or $\mu_2\epsilon_2$ is decreased sufficiently. When α is zero, equations (B1) to (B6) show that the fields revert to plane waves traveling parallel to the sheet. Therefore, any combination of parameters, t , ω , or $\mu_2\epsilon_2$ which cause α to go to zero for a given surface-wave mode is sufficient to define the cut-off conditions for that mode.

Applying the boundary conditions to equations (B1) to (B6) gives the following relationships:

$$\alpha \frac{\mu_2}{\mu_1} = k \tan\left(\frac{kt}{2} - \frac{m\pi}{2}\right) \quad (\text{B7})$$

$$\alpha \frac{\epsilon_2}{\epsilon_1} = k \tan\left(\frac{kt}{2} - \frac{m\pi/2}{2}\right) \quad (\text{B8})$$

$$\alpha^2 - h^2 = -\omega^2 \mu_1 \epsilon_1 \quad (\text{B9})$$

$$k^2 + h^2 = \omega^2 \mu_2 \epsilon_2 \quad (\text{B10})$$

APPENDIX B

by using equations (B7) and (B8) at cutoff (that is, $\alpha = 0$)

$$\tan\left(\frac{kt}{2} - \frac{m\pi}{2}\right) = 0 \quad (\text{B11})$$

or

$$\frac{kt}{2} = \frac{m\pi}{2} \quad (\text{B12})$$

and

$$h = \omega^2 \mu_1 \epsilon_1 \quad (\text{B13})$$

$$k^2 = \omega^2 (\mu_2 \epsilon_2 - \mu_1 \epsilon_1) \quad (\text{B14})$$

Therefore, using equations (B12) and (B14) gives a cutoff

$$\frac{\omega t}{2} \sqrt{\mu_2 \epsilon_2 - \mu_1 \epsilon_1} = \frac{m\pi}{2} \quad (\text{B15})$$

since

$$\omega = 2\pi f = \frac{2\pi}{\lambda_1 \sqrt{\mu_1 \epsilon_1}} \quad (\text{B16})$$

Substituting equation (B16) into equation (B15) and denoting μ_2/μ_1 by μ_r' and ϵ_2/ϵ_1 by ϵ_r' gives

$$\frac{t}{\lambda_1} = \frac{m}{2\sqrt{\mu_r' \epsilon_r' - 1}} \quad (\text{B17})$$

For $m = 0$, $\frac{t}{\lambda_1} = 0$; thus, for any thickness of the dielectric, the TE_0 and TM_0 surface-wave modes are not cut off.

Consider that a thin conducting sheet is inserted in the y', z' plane. The same field conditions apply except that t is twice the thickness used in the cutoff conditions of equation (B17), that is (λ_1 being replaced by λ_v)

$$\frac{T_0}{\lambda_0} = \frac{m}{4\sqrt{\mu_r' \epsilon_r' - 1}} \quad (\text{B18})$$

In addition, all even TE modes and odd TM modes cannot exist.

APPENDIX B

Calculations. - By utilizing the cutoff condition given in equation (B18), calculations can be made to determine the modes that exist for particular values of μ_r' , ϵ_r' , and λ_v . For the case at hand, $\mu_r' = 1$, $\epsilon_r' = 2.54$, and $\lambda_v = 1.28$ inches. A partial list of the modes that can exist and their corresponding cutoff thicknesses T_0 are given:

Mode number	Cutoff thickness, T_0 , in. (cm)
TM ₀	0 (0)
TE ₁	0.2585 (0.657)
TM ₂	0.5170 (1.313)
TE ₃	0.7755 (1.970)
TM ₄	1.0340 (2.626)

For reference, the thicknesses of maximum and minimum reflection for a plane dielectric sheet with an incident plane wave at normal incidence are: $\frac{T}{\lambda\epsilon} = \frac{\lambda\epsilon}{4} = 0.2012$ inch (0.51 cm), $\frac{T}{\lambda\epsilon} = \frac{\lambda\epsilon}{2} = 0.4024$ inch (1.01 cm), $\frac{T}{\lambda\epsilon} = \frac{3\lambda\epsilon}{4} = 0.6036$ inch (1.53 cm), and $\frac{T}{\lambda\epsilon} = \lambda\epsilon = 0.8048$ inch (2.04 cm). It should be noted that none of the reflection conditions and surface wave cutoff conditions coincide.

Application

Reference should be made to figure 2(b), which depicts the slot on a coated cylinder geometry. Consider a slot centered on the x-axis at $z = 0$. Also consider that the pattern of interest will be observed in the ϕ -plane ($\theta = 90^\circ$). To apply the surface wave results to this case, it will be necessary to consider the cylinder locally plane so that the following coordinates are aligned: $+y' = z$, $x' = x$, $-z' = y$. The slot thus will, depending upon T , excite surface waves in both the z-direction (TM_m) and in the ϕ -plane (TE_n). Since the patterns under consideration are in the ϕ -plane, only the TE_n surface wave modes are of interest. It should be noted that the slot will by symmetry excite a traveling wave in both the $\mp y = \mp z'$ directions.

It should be noted at this point that patterns were computed and measured that include dielectric thicknesses above cutoff for the TE₁, TE₃, and TM₀ modes.

Pattern Ripples

Reference should be made to figure 6 and, in particular, to the changes in pattern shape as a function of thickness. There appears to be little difference from the uncoated case through $T = 0.1616$ inch (0.41 cm). For $T = 0.1934$ inch (0.49 cm) and $T = 0.2262$ inch (0.57 cm), the pattern appears to broaden; however, ripples do not

APPENDIX B

appear until $T = 0.2585$ inch (0.66 cm). After this thickness the ripples increase in amplitude until $T = 0.3555$ inch (0.90 cm) and then diminish. The patterns again resemble the free-space pattern until $T = 0.7091$ inch (1.80 cm) where the patterns again broaden. Ripples do not appear again until $T = 0.7755$ inch (1.97 cm).

It should now be noted that the patterns where ripples first occur, $T = 0.2585$ inch (0.66 cm) and $T = 0.7755$ inch (1.97 cm) correspond identically to the cutoff thickness of the TE_1 and TE_3 plane surface-wave modes.

Similar observations can be made concerning the measured patterns, allowance being made for the recessed channel effects.

Results

Based upon the previous discussion and calculations, a qualitative explanation of the pattern behavior in figures 6 and 9 is now stated in the succeeding statements.

For the uncoated cylinder of such large circumference, the observed radiation field is the result of currents $J_z(\phi)$ excited by the slot as illustrated in figure 14(a). However, the amplitude of such currents decreases rapidly as a function of ϕ such that no significant amplitude exists at the shadow boundaries $\phi = 90^\circ$ and $\phi = 270^\circ$. Hence, there is no significant radiation in the side opposite the slot or so-called shadow region.

With the introduction of a dielectric layer, however, a more complex equivalent current structure is possible. Because of trapping, currents of significant amplitude can exist to the shadow boundary and beyond, as depicted in figure 14(b). However, the strengths of such currents beyond those set up in the uncoated case are critically dependent upon the excitation or coupling of slot energy into the layer. No theory is presently available to predict such coupling for this particular case; however, an inferred strength is discussed later.

Thus, the character of the patterns observed in the coated case can be generally predicted by utilizing the following physical model. The nature of the power flow in the general coated case is depicted by rays in figure 15. Radiation of the surface-wave energy will be approximately tangential to the local normal. Therefore, in the far field of the cylinder on the shadow side, the observed field will always appear as two sources located approximately $2a$ apart. The amplitudes of the sources will vary depending upon observation angle; however, the phase relationship will remain fixed. By utilizing simple array theory, the angular distance between phase additions was calculated to be approximately 4° . This angular separation between lobes was observed in the shadow region for all experimental and theoretical patterns where ripples were observed.

A qualitative indication of the surface wave launching efficiency in this case can be inferred from the patterns of figure 6. For a thickness of $T < 0.2585$ inch (0.66 cm),

APPENDIX B

no appreciable energy can be coupled into the dielectric layer; therefore no energy is coupled to the shadow boundary and no ripples are observed. At $T = 0.2585$ inch (0.66 cm), which corresponds to the cutoff at the TE_1 mode, some energy is coupled into the layer. However, the energy is weakly bound and the coupling to the slot is weak. Thus, only limited rippling is observed. For $T > 0.2585$ inch (0.66 cm), more energy is coupled into the layer and the energy is increasingly bound to the surface. This results in both higher amplitude of ripples and a wider angular extent. At some thickness (about $T = 0.5494$ inch (1.40 cm)), the coupling of slot energy into the layer decreases nearly to zero, and even though the TE_1 surface wave mode can freely propagate, no appreciable energy is coupled into it. This condition persists until $T = 0.7755$ inch (1.97 cm), which is the cutoff thickness for the TE_3 mode, where ripples again appear in the patterns.

Based upon the foregoing discussion, the designer of such slot arrays as considered in this paper has two positive methods of avoiding the "critical thickness" for a particular set of design parameters a , λ_v , ϵ_r' , and T variable. By utilizing equation (5) he can compute the element pattern to ascertain the existence of ripples. This procedure, however, requires considerable computational effort. Alternately, he can compute the cutoff thicknesses of the TE_m surface-wave modes by using equation (B18). Preferably, a coating thickness equal to or less than the cutoff thickness of the TE_1 mode is utilized. Alternately, thicknesses equal to the cutoff thicknesses of the higher TE_m modes should be utilized.

APPENDIX C

THE DESIGN OF SHUNT SLOTS IN THE BROAD WALL OF A WAVEGUIDE COVERED BY A DIELECTRIC LAYER

The purpose of this appendix is to review concisely the design of dielectric-covered shunt slots in a waveguide (refs. 6 and 18). The effects of the recessing channel are neglected in this discussion. In these experimental studies (refs. 6 and 18), slot lengths and displacements were chosen so that the peak normalized conductance g_s had the range of $0.029 \leq g_s \leq 0.115$ and resonant slot lengths corresponding to resonant frequencies from 10.8 GHz to 12.4 GHz. By utilizing RG-52/U waveguide and standard measurement techniques (ref. 19), conductances were measured for dielectric constants of $1 \leq \epsilon_r' \leq 4$ and thicknesses of $0.095 \leq T \leq 0.950$ inch. A typical set of data is given in figure 16. A study of the data revealed that gross changes in slot characteristics can occur with the addition of a dielectric layer. However, the slots do maintain a resonant behavior, although their peak conductance is greatly reduced. The essential changes in slot characteristics can be summarized in the following observations:

(1) The frequency at which resonance occurs (defined as the frequency at peak conductance) decreases radically as a function of dielectric thickness T up to $T = 0.20\lambda$ ($\lambda = \lambda_v / \sqrt{\epsilon_r'}$). For $T \gtrsim 0.20\lambda$, the resonant frequency deviates slightly about a mean value f_R .

(2) A significant reduction of normalized conductance occurs with the addition of a dielectric cover for thicknesses up to $T \approx 0.2\lambda$. For $T \gtrsim 0.20\lambda$, the peak conductance varies approximately sinusoidally about a mean value.

(3) The resonant conductance is much lower than that predicted for a slot with no cover.

By restricting attention to dielectric layers where $T \gtrsim 0.2\lambda$, the following comments concerning design can be made:

(1) An average or mean resonant frequency f_R can be found which is dependent upon ϵ_r' and independent of layer thickness and slot displacement. Such a value of f_R is denoted in figure 16. Values of f_R and its associate wavelength $\lambda_R = c/f_R$ were obtained for all the cases measured and were converted to equivalent resonant slot length ratios l_R/λ_R . It is then assumed that if with the same dielectric coating condition at the free space wavelength λ_v , the slot length is reduced to a value l_v such that $\frac{l_v}{\lambda_v} = \frac{l_R}{\lambda_R}$, the slot would still be resonant. That this is so was substantiated by measurement. Figure 8 summarizes these experimental data. With a knowledge of the

APPENDIX C

desired operating frequency λ_v and layer dielectric constant ϵ_r' , one can then determine from figure 8 the required slot length l to obtain a resonance length accurate to about ± 5 percent.

(2) An approximate expression for the conductance g of a resonant slot coated with a layer of dielectric constant ϵ_r' and of thickness $T \gtrsim 0.2\lambda$ (and, therefore, having a length as determined by fig. 8) which is related to the slot conductance g_v or a noncoated resonant slot at the same frequency (this slot will hence be longer, as determined by fig. 8) can be derived which is independent of layer thickness. This is done by assuming the waveguide and slot to be equivalent to a constant current source I operating into the radiation resistance R_c . The power coupled out of such a slot P is given by (ref. 14).

$$P = \frac{I^2}{(2)(73)} \frac{\mu_v}{\epsilon_v \epsilon_r'} = IR_c \quad (C1)$$

Equation (C1) assumes the half space outside the waveguide to be filled with a material with dielectric constant ϵ_r' . This assumption is approximately true for $T \gtrsim 0.2\lambda$, since for such thickness the measured conductance was substantially constant and tended to oscillate about a mean value. If P_v is the power coupled out of the slot resonant with external medium $\mu_v \epsilon_v$, and P is the power coupled out of the slot resonant with an external medium $\mu_v \epsilon_v \epsilon_r'$, for equal currents

$$P = \frac{P_v}{\epsilon_r'} \quad (C2)$$

or the relationship between the radiation resistance of the two resonant slots in the coated R_c and noncoated R_{cv} condition is

$$\frac{R_c}{R_{cv}} = \frac{1}{\epsilon_r'} \quad (C3)$$

or, in terms of the external radiation conductances $\left(G_{cv} = \frac{1}{R_{cv}}; \quad G_c = \frac{1}{R_c} \right)$

$$\frac{G_c}{G_{cv}} = \epsilon_r' \quad (C4)$$

By following the method of Stevenson (ref. 12), a relationship between the equivalent waveguide normalized (with respect to the waveguide admittance) resonant slot conductances for the coated g_s and uncoated g_v cases can be obtained as follows (from ref. 20).

APPENDIX C

The magnetic field along the slot is assumed to be that of the dominant TE_{10} mode. That is $H_0 e^{-j\beta z} \sin\left(\frac{\pi x_S}{x_0}\right)$; the electric field across the slot is taken as $E_0 \cos\left(\frac{\pi z}{l}\right)$ since the slot is resonant, where E_0 is as yet unknown and $H_0 = H_0^+(1 + \Gamma)$ where H_0^+ is the incident axial magnetic field. The reflection coefficient is Γ , and is assumed to be real at resonance. The power radiated by the slot is then

$$P = - \int_{-l/2}^{l/2} \frac{w}{2} E_0^* \cos \frac{\pi z}{l} H_0 e^{+j\beta z} \sin \frac{\pi x_S}{x_0} dz = - \frac{V_0^* H_0}{2} I \sin \pi \frac{x_S}{x_0} \quad (C5)$$

where

$$I = \int_{-l/2}^{l/2} \cos \frac{\pi z}{l} e^{-j\beta z} dz \quad (C6)$$

and where $V_0 = E_0 w =$ voltage across the center of the slot. Now, by definition the external radiation conductance G_c is

$$G_c \equiv \frac{2P}{|V_0|^2} \quad (C7)$$

Using equation (C7) to solve for V_0 in terms of G_c and P and inserting the results into equation (C5) gives

$$P = \frac{|H_0|^2 |I|^2}{2G_c} \sin^2 \frac{\pi x_S}{x_0} \quad (C8)$$

If a short circuit is placed a quarter of a guide wavelength from the center of the slot, the power P can also be expressed in terms of the waveguide quantities

$$P = P^+(1 + \Gamma)(1 - \Gamma^*) \quad (C9)$$

where P^+ is the incident power in the TE_{10} mode, and Γ is the reflection coefficient

$$P^+ = |H_0^+|^2 \eta_v \frac{x_0^3 y_0}{\lambda_g \lambda_v} \quad (C10)$$

with

$$\eta_v = \sqrt{\mu_v / \epsilon_v}$$

APPENDIX C

Equations (C8) and (C9), with $\Gamma = \Gamma^*$, gives g_S as

$$g_S = \frac{1 - \Gamma}{1 + \Gamma} = \frac{\lambda_g \lambda_v |I|^2}{2 \eta_v x_O^3 y_O G_C} \sin^2 \left(\frac{\pi x_S}{x_O} \right) \quad (C11)$$

Thus, with equations (C11) and (C4), one obtains

$$\frac{g_S}{g_V} = \frac{1}{\epsilon_r} \frac{|I|^2}{|I_v|^2} \quad (C12)$$

Evaluation of $|I|^2$ gives

$$|I|^2 = \frac{4l^2 \cos^2 \left(\frac{\pi l}{\lambda_g} \right)}{\eta^2 \left(1 - \frac{4l^2}{\lambda_g^2} \right)} \quad (C13)$$

and evaluating equation (C11) for the noncoated case $(l = \frac{\lambda_v}{2})$ given Stevenson's result (ref. 12)

$$g_V = 2.09 \frac{\lambda_g x_O}{\lambda_v \lambda_O} \cos^2 \frac{\pi}{2} \frac{\lambda_v}{\lambda_g} \sin^2 \pi \frac{x_S}{x_O} \quad (C14)$$

Hence, equation (C12) gives

$$g_S = K \sin^2 \pi \frac{x_S}{x_O} \quad (C15)$$

$$K = \frac{8.36}{\epsilon_r} \left(\frac{l}{\lambda_v} \right)^2 \left[\frac{1 - \left(\frac{\lambda_v}{\lambda_g} \right)^2}{1 - 4 \left(\frac{\lambda_v}{\lambda_g} \right)^2 \left(\frac{l}{\lambda_v} \right)^2} \right]^2 \cos^2 \left[\pi \frac{\lambda_v}{\lambda_g} \left(\frac{l}{\lambda_v} \right) \right] \left(\frac{\lambda_g x_O}{\lambda_v y_O} \right) \quad (C16)$$

where the resonant length l/λ_v is determined from figure 8 for $\epsilon_r' = 1$ and for any $1 \leq \epsilon_r' \leq 4$ and $T \gtrsim 0.2\lambda$.

It should be noted that the recess used in the array design for pattern control may affect the slot impedance in such a way that a final tuning adjustment may be necessary.

REFERENCES

1. Croswell, W. F.; and Knop, C. M.: On the Use of an Array of Circumferential Slots on a Large Cylinder as an Omnidirectional Antenna. *IEEE Trans. Antennas Propagation*, vol. AP-14, no. 3, May 1966, pp. 394-396.
2. Cockrell, C. R.; and Croswell, W. F.: The Application of Circular Arrays to Spacecraft Antenna Problems. *IEEE Trans. Aerospace*, vol. AS-2, no. 2, Apr. 1964, pp. 272-277.
3. Wait, James R.: *Electromagnetic Radiation From Cylindrical Structures*. Pergamon Press, 1959.
4. Knop, C. M.: The Radiation Fields From a Circumferential Slot on a Metal Cylinder Coated with a Lossy Dielectric. *IRE Trans. Antennas and Propagation*, vol. AP-9, no. 6, Nov. 1961, pp. 535-545.
5. Knop, Charles M.; and Cohn, George I.: Radiation From an Aperture in a Coated Plane. *Radio Sci. J. Research, MBS/USNC - URSI*, vol. 68D, no. 4, Apr. 1967, pp. 363-378.
6. Croswell, W. F.; and Higgins, R. B.: A Study of Dielectric Covered Shunt Slots in a Waveguide. *IEEE, Trans. Aerospace*, Vol. AS-2, no. 2, Apr. 19, 1964, pp. 278-283.
7. Knudsen, H. L.: Radiation from Ring Quasi-Arrays. *IRE Trans. Antennas Propagation*, vol. AP-4, no. 3, July 1956, pp. 452-472.
8. Chu, Ta-Shing: On the Use of Uniform Circular Arrays To Obtain Omnidirectional Patterns. *IRE Trans. on Antennas and Propagation*, vol. AP-7, no. 4, Oct. 1959, pp. 436-438.
9. Jordan, Edward C.: *Electromagnetic Waves and Radiating Systems*. Prentice Hall, Inc., 1950.
10. Jasik, Henry, ed.: *Antenna Engineering Handbook*. McGraw-Hill Book Co., Inc., 1961.
11. Watson, W. H.: *The Physical Principles of Wave Guide Transmission and Antenna Systems*. Clarendon Press (Oxford), 1947.
12. Stevenson, A. F.: Theory of Slots in Rectangular Wave-Guides. *J. Appl. Phys.*, vol. 19, no. 1, Jan. 1948, pp. 24-38.
13. Ramsay, John F.; and Popovich, Boris V.: Series-Slotted Waveguide Array Antennas. 1963 IEEE International Convention Record. Part 1.- Antennas and Propagation, Mar. 1963.
14. Harrington, Roger F.: *Time-Harmonic Electromagnetic Fields*. McGraw-Hill Book Co., Inc., 1961.

15. Mueller, G. E., and Tyrrell, W. A.: Polyrod Antennas. Bell System Tech. J., vol. XXVI, no. 4, Oct. 1947, pp. 837-851.
16. Barlow, H. M.; and Brown, J.: Radio Surface Waves. The Clarendon Press (Oxford), c.1962.
17. Richmond, J. H.: Reciprocity Theorems and Plane Surface Waves. Bull. no. 176, Eng. Expt. Sta., Ohio State Univ. Studies, vol. XXVIII, no. 4, July 1959.
18. Croswell, William F.; and Higgins, Robert B.: Effects of Dielectric Covers Over Shunt Slots in a Waveguide. NASA TN D-2518, 1964.
19. Thourel, L. (Translated by H. deLarstre Banting): The Antenna. John Wiley & Sons, Inc., c.1956.
20. Knop, C. M.; Hodara, H.; Butler, L.; Gilon, P.; Love, A. W.; and Rasmussen, G.: Final Report – Research Study of Some Ram Antennas. SN 226 (Contract NAS1-4623), Nat. Eng. Sci. Co., June 1965.

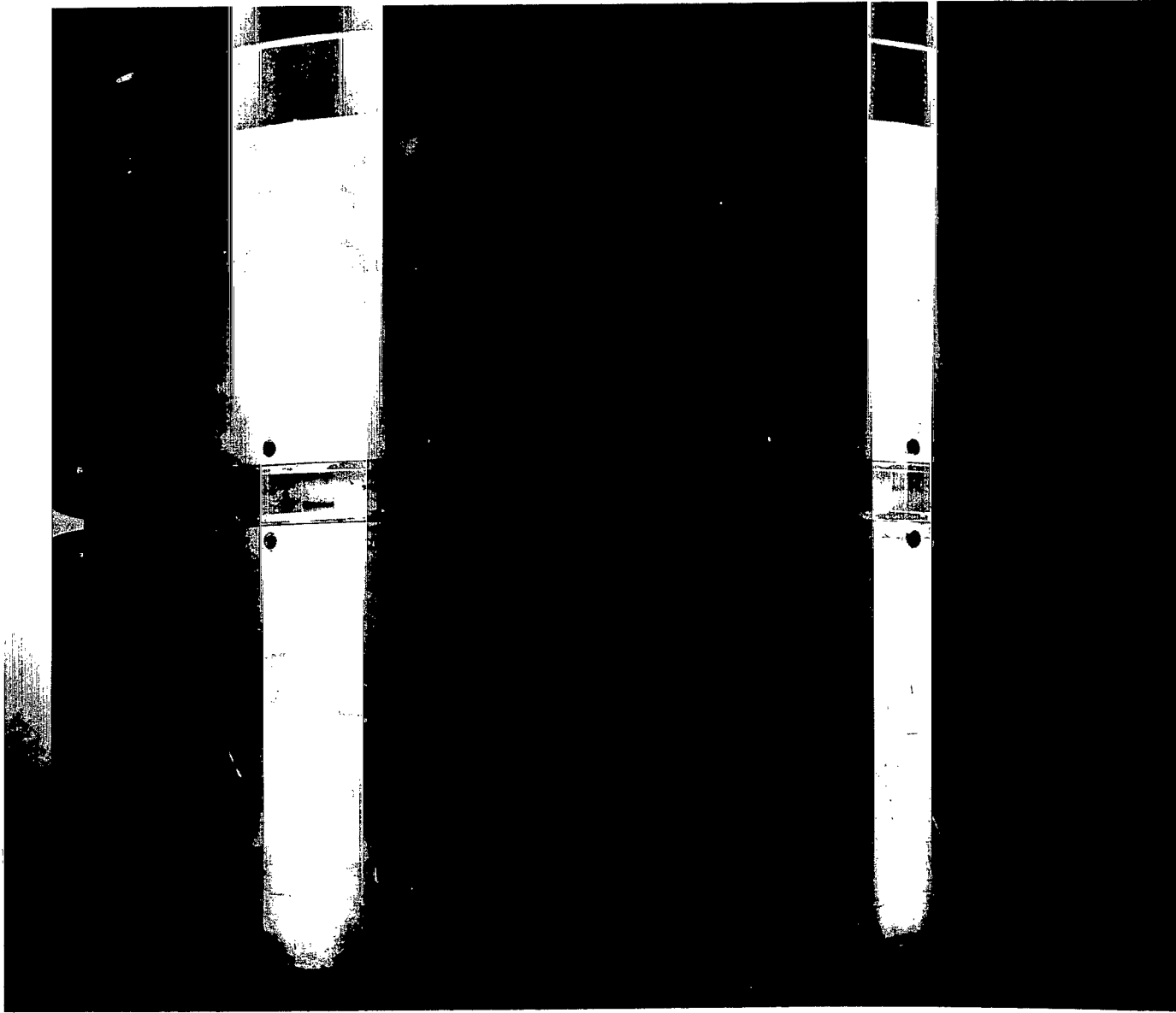


Figure 1.- Photograph of dielectric-coated circular array of shunt slots in a waveguide.

L-66-7116

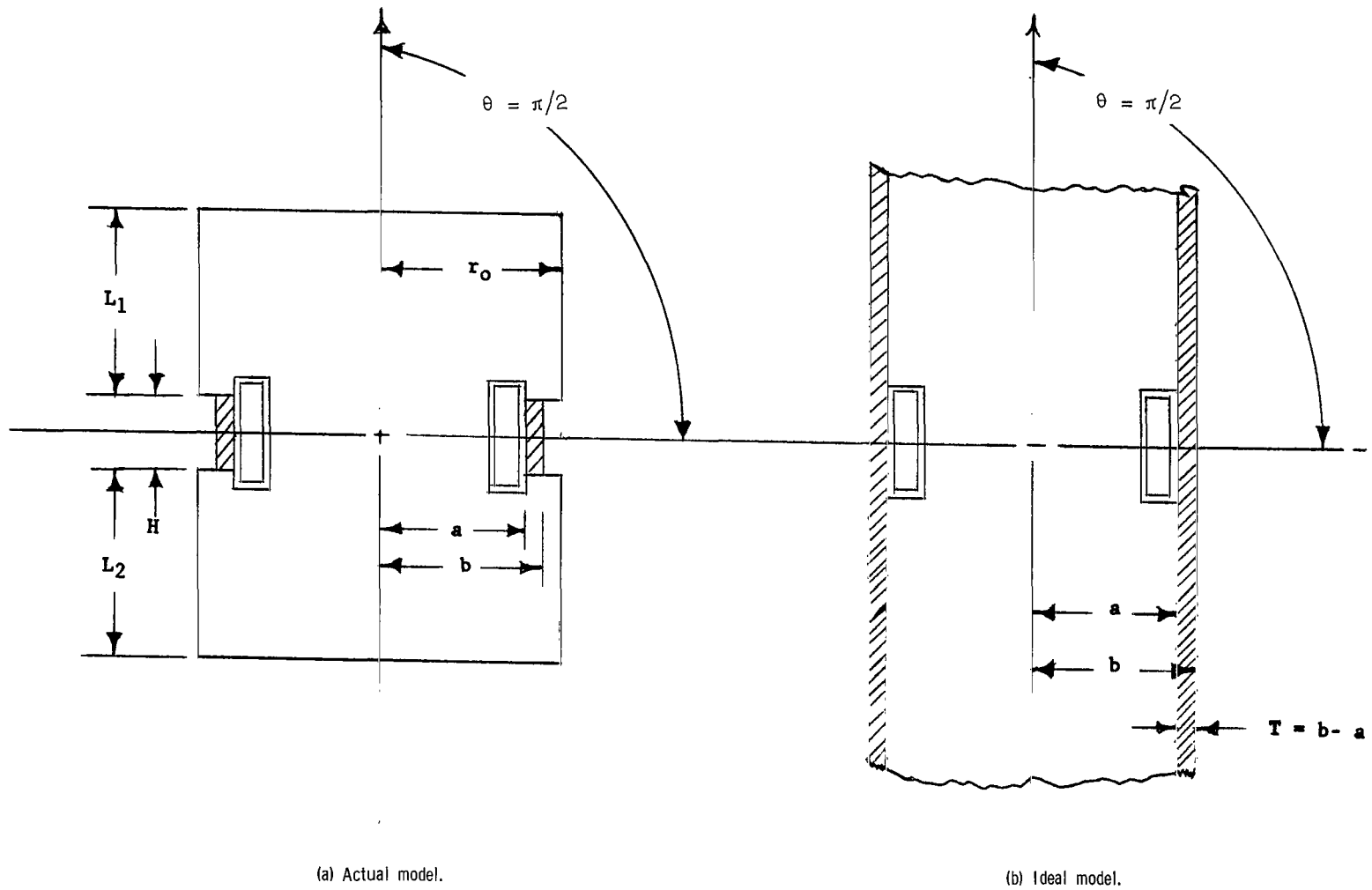


Figure 2.- Ring waveguide slot array.

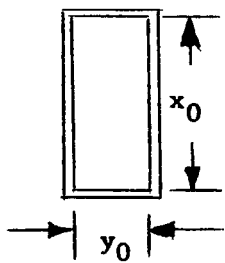
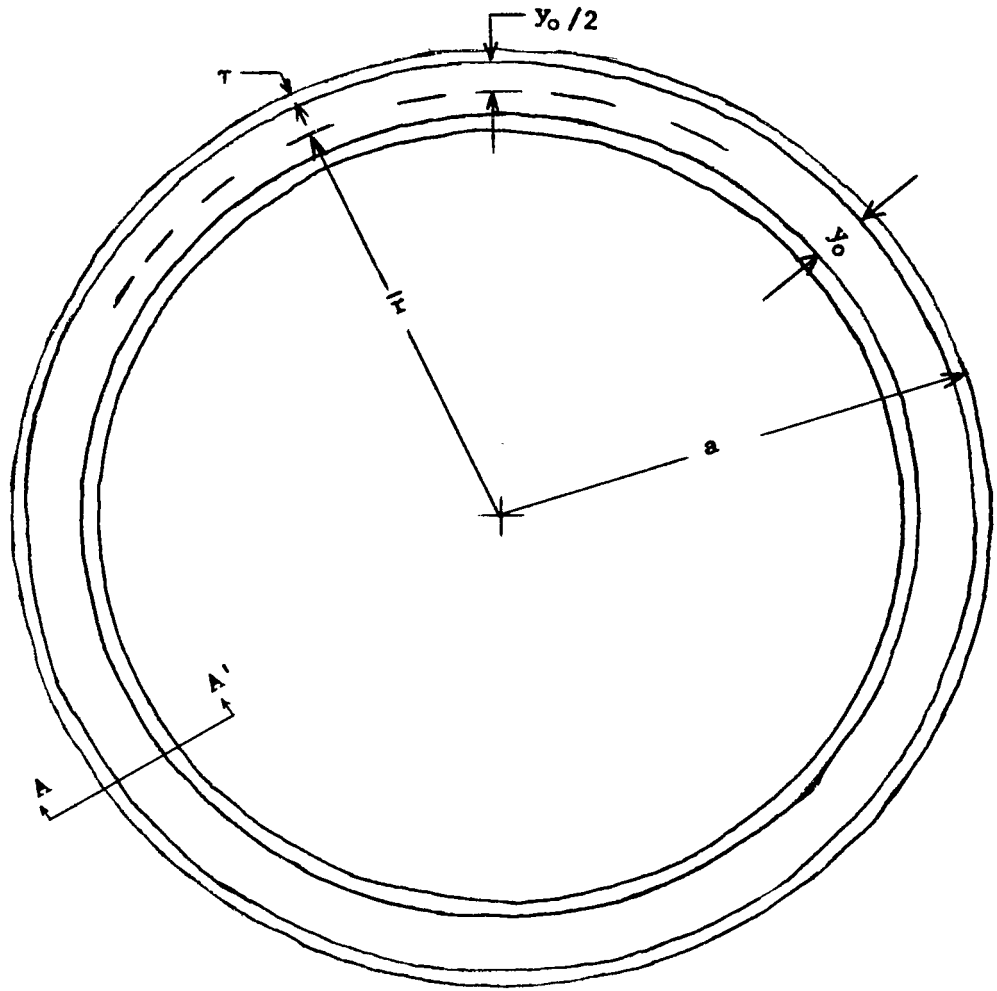
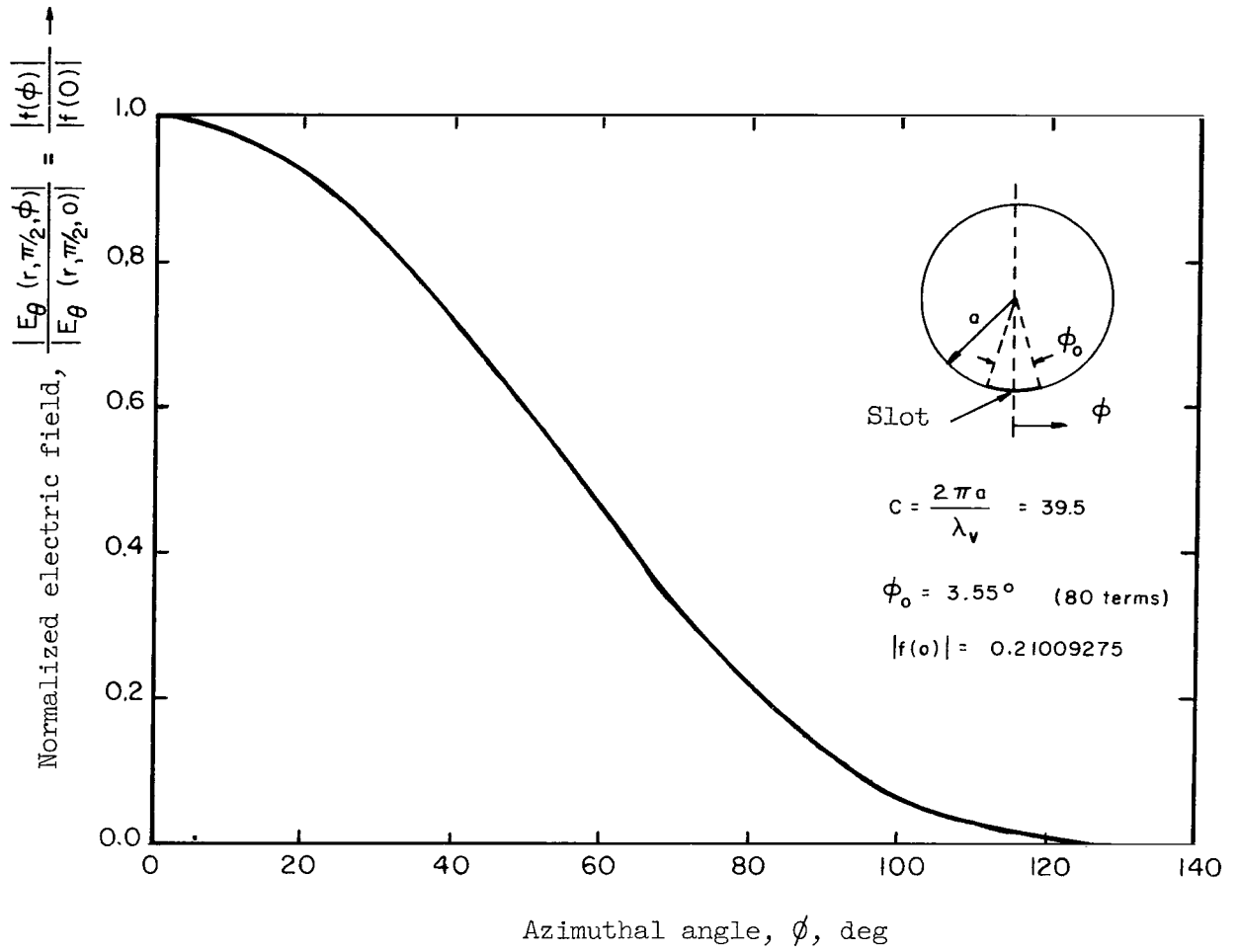
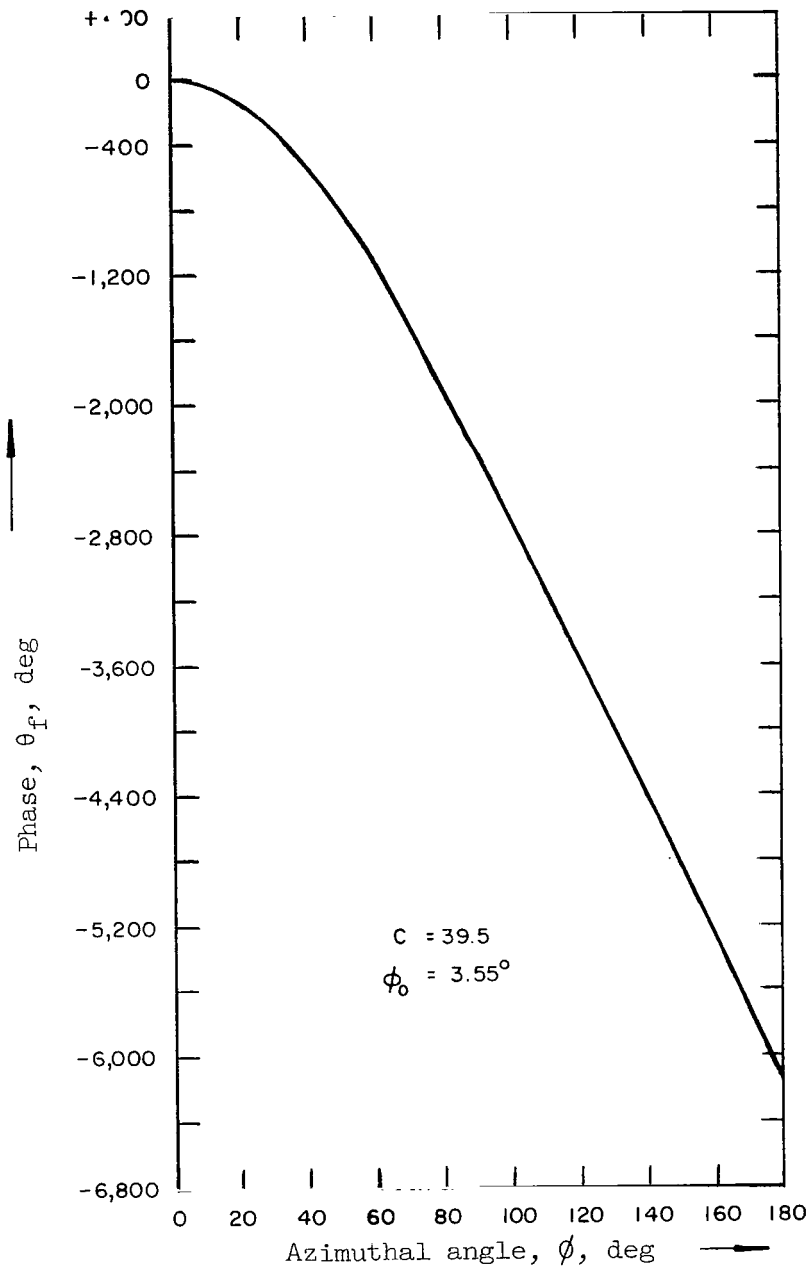


Figure 3.- Ring waveguide.



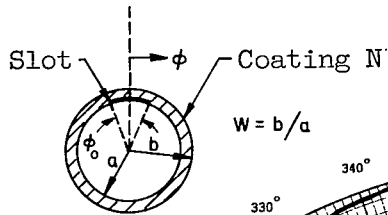
(a) Amplitude.

Figure 4.- Computed equatorial pattern for a single circumferential slot. No coating.



(b) Phase.

Figure 4.- Concluded.



For all patterns

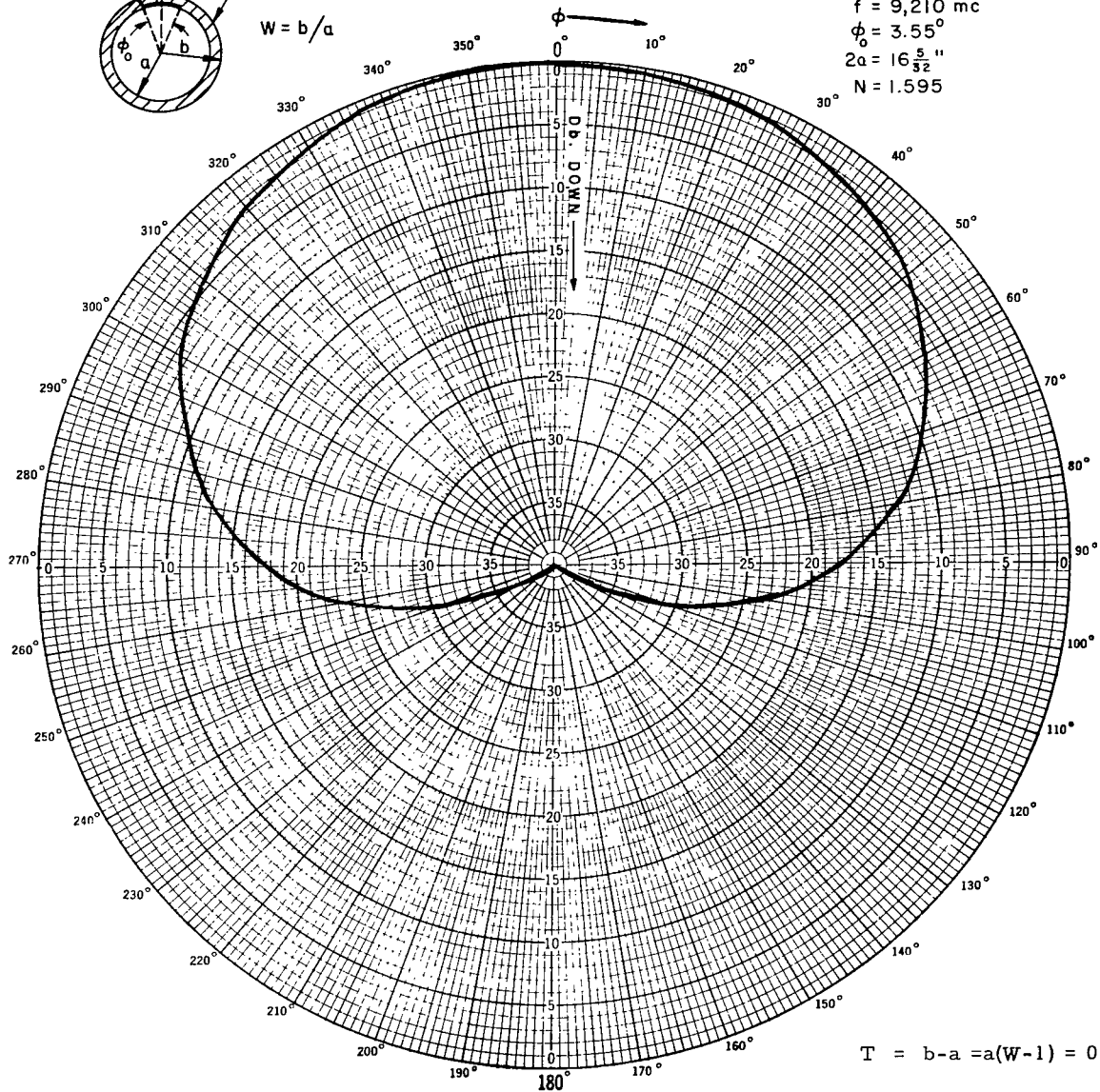
$$C = 39.5 = 2\pi a / \lambda_v$$

$$f = 9,210 \text{ mc}$$

$$\phi_0 = 3.55^\circ$$

$$2a = 16 \frac{5}{32} \text{ ''}$$

$$N = 1.595$$

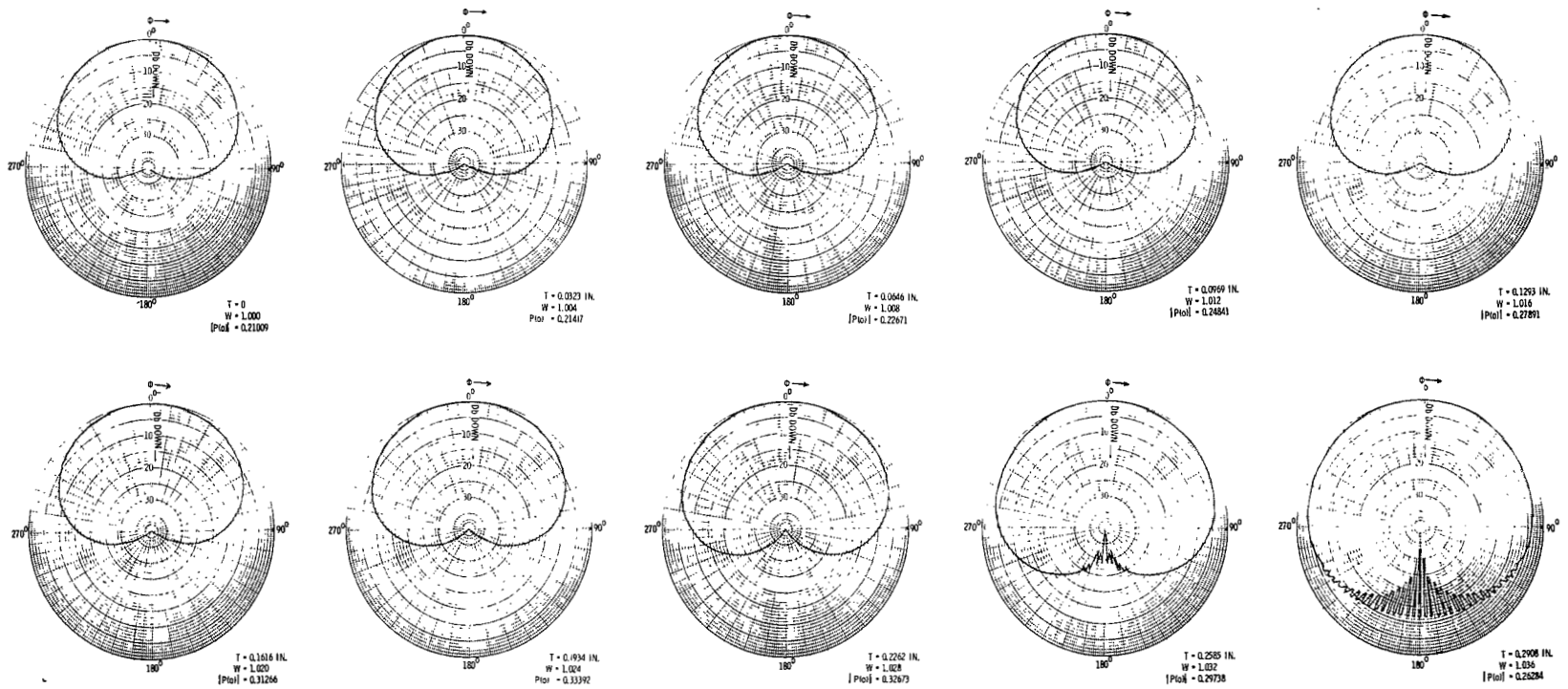


$$T = b - a = a(W - 1) = 0$$

$$W = 1.000$$

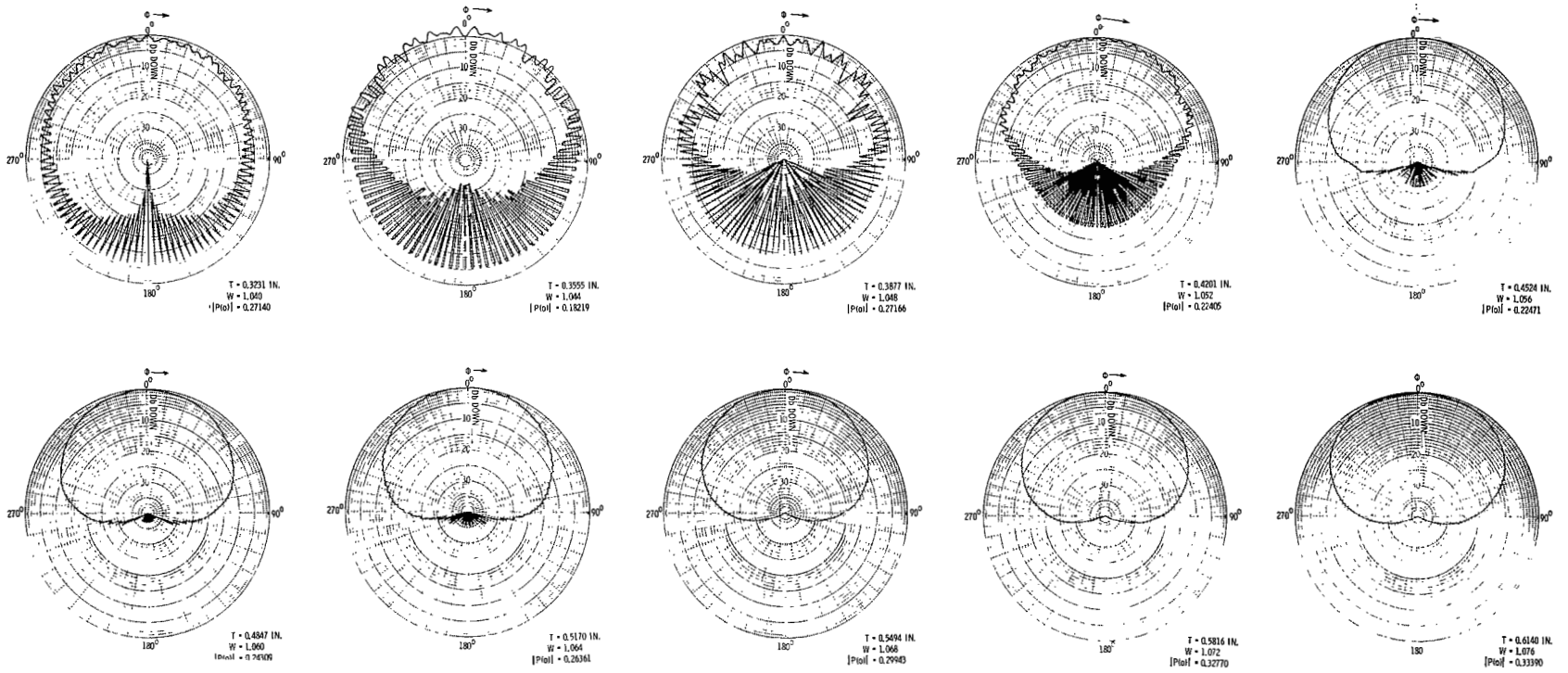
$$|P(\phi)| = 0.21009$$

Figure 5.- Computed equatorial plane pattern of a single circumferential slot. No coating.



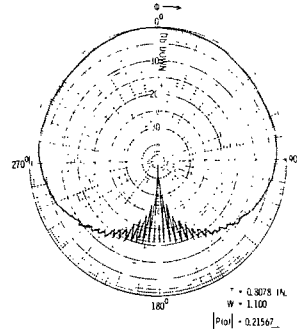
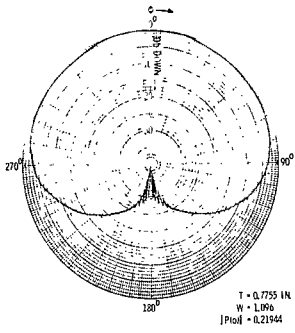
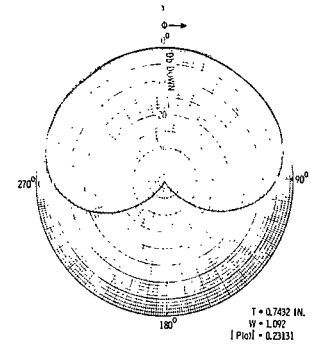
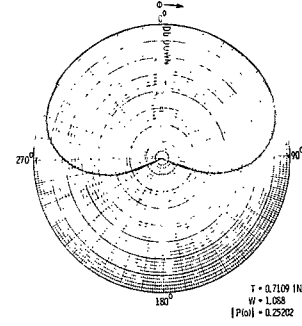
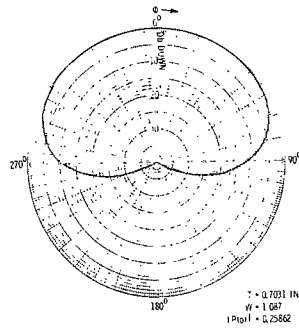
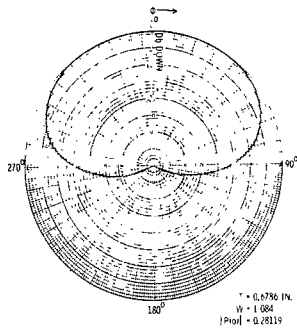
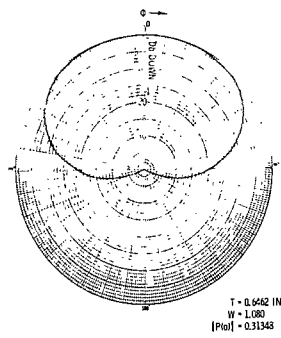
(a) $T = 0$ inch (0.00 cm) to $T = 0.2908$ inch (0.7386 cm).

Figure 6.- Computed equatorial power pattern of a single circumferential slot.



(b) $T = 0.3231$ inch (0.8207 cm) to $T = 0.6140$ inch (1.560 cm).

Figure 6.- Continued.



(c) $T = 0.6462 \text{ inch (1.641 cm)}$ to $T = 0.8078 \text{ inch (2.052 cm)}$.

Figure 6.- Concluded.

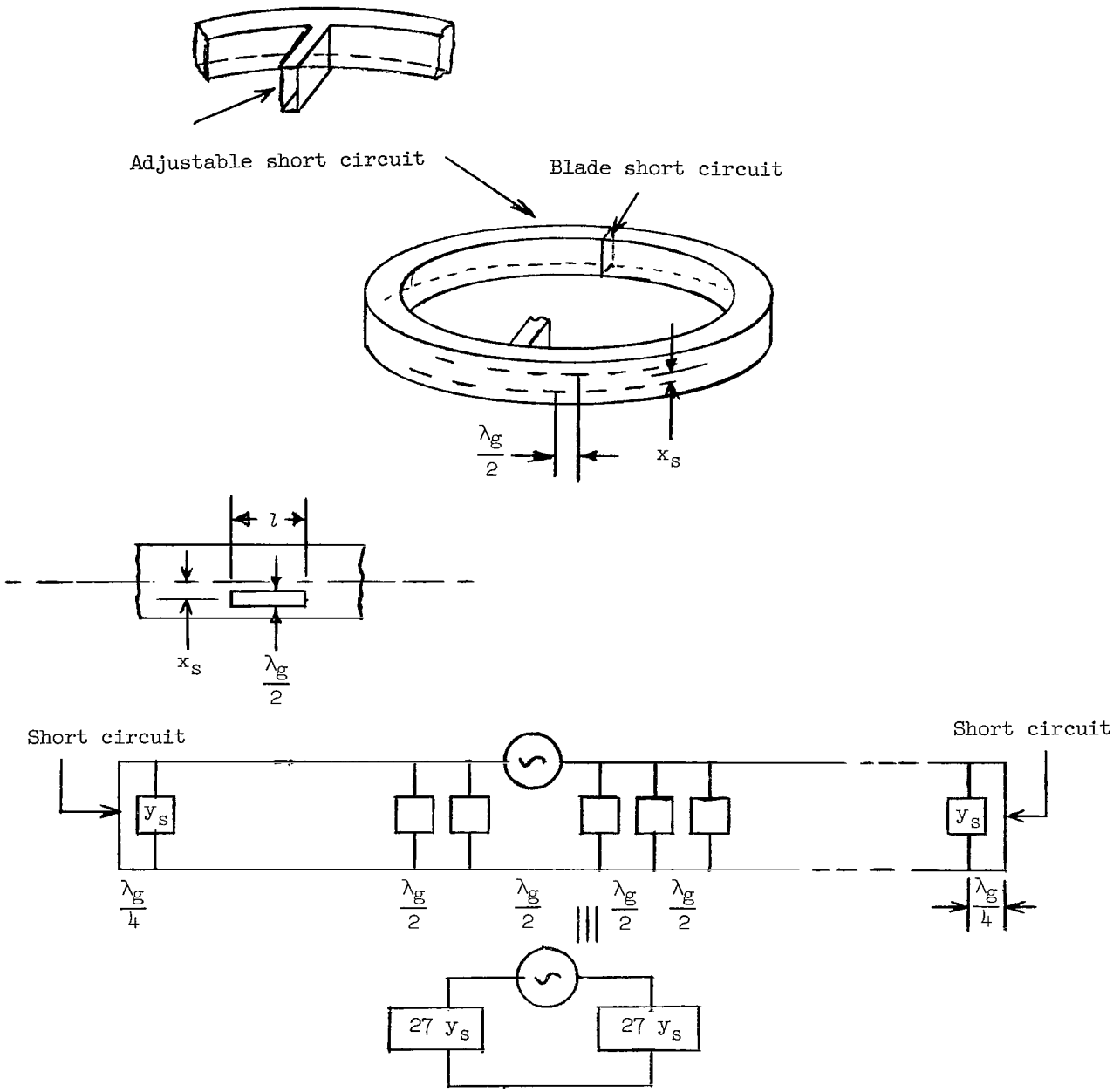


Figure 7.- Ring resonant waveguide array, feed arrangement, and equivalent circuit.

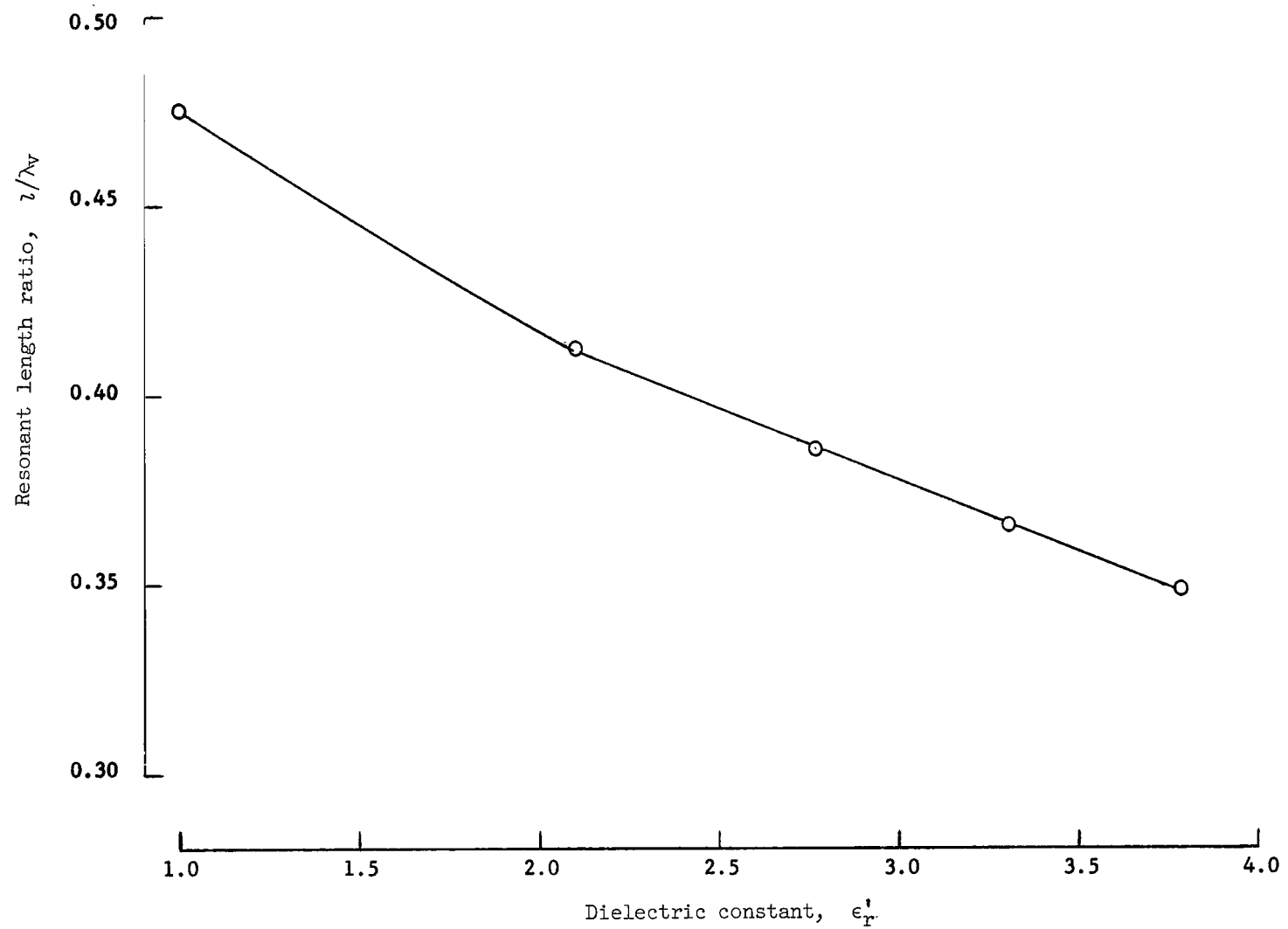
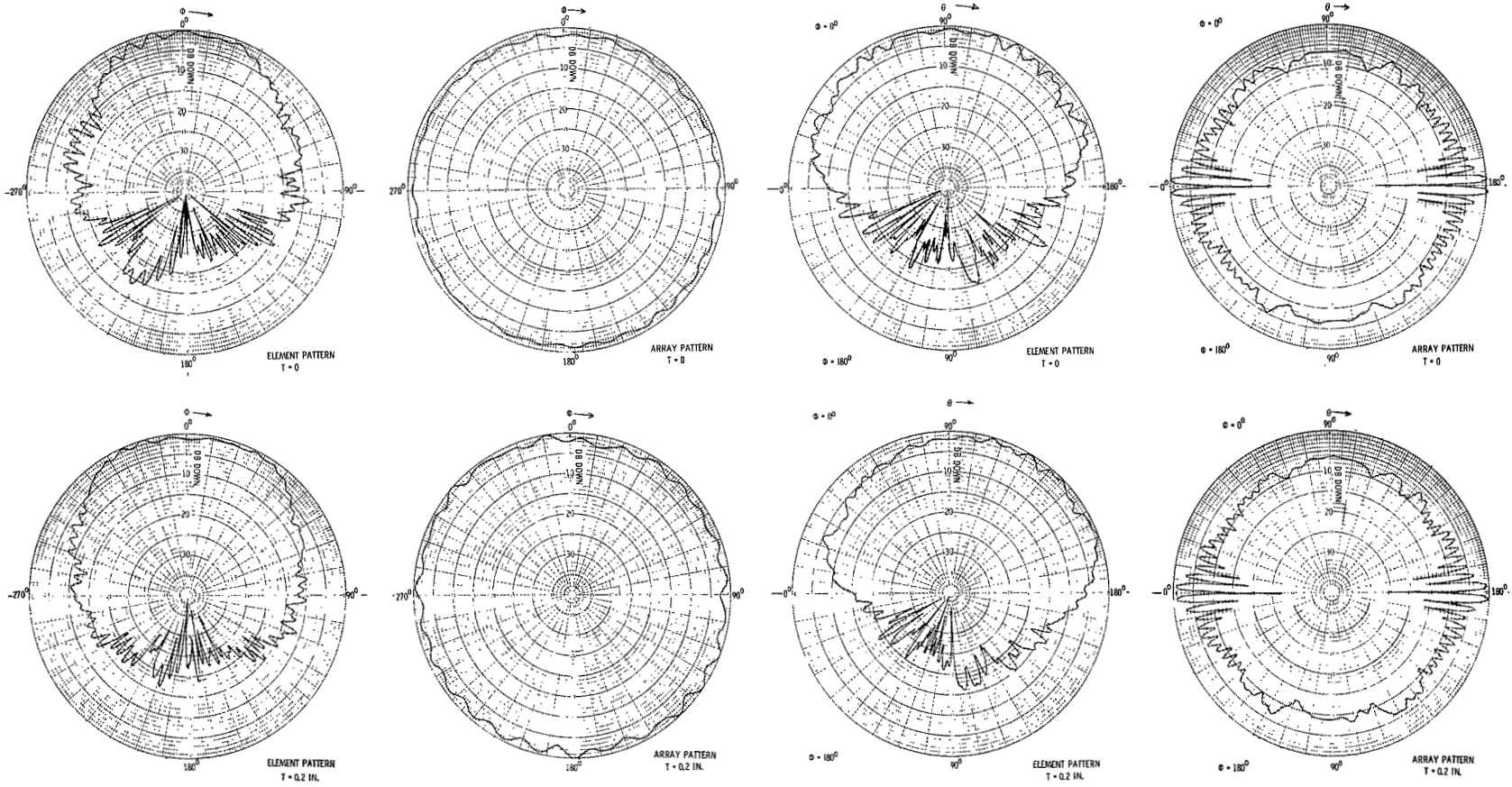
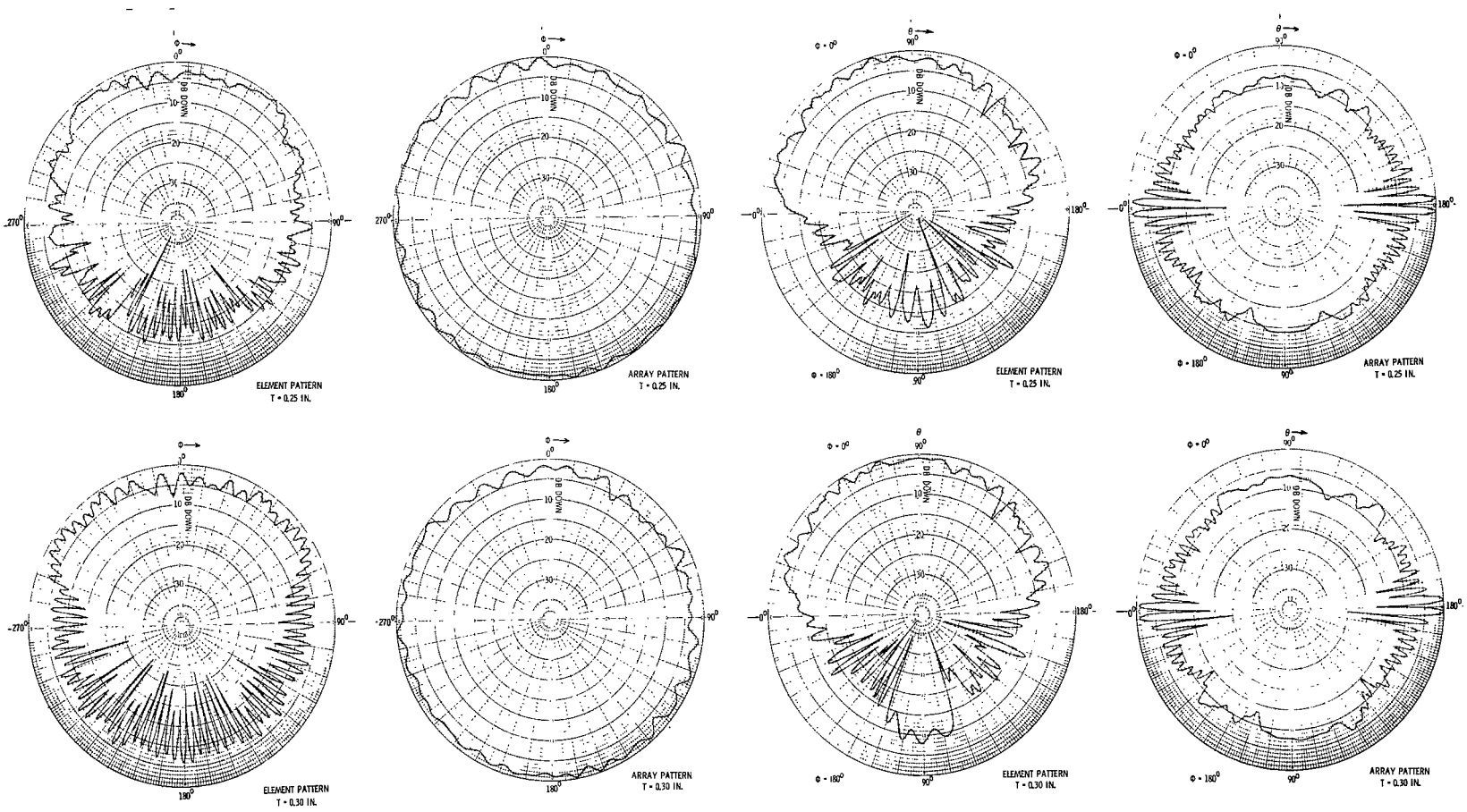


Figure 8.- Resonant length ratio as a function of dielectric constant.



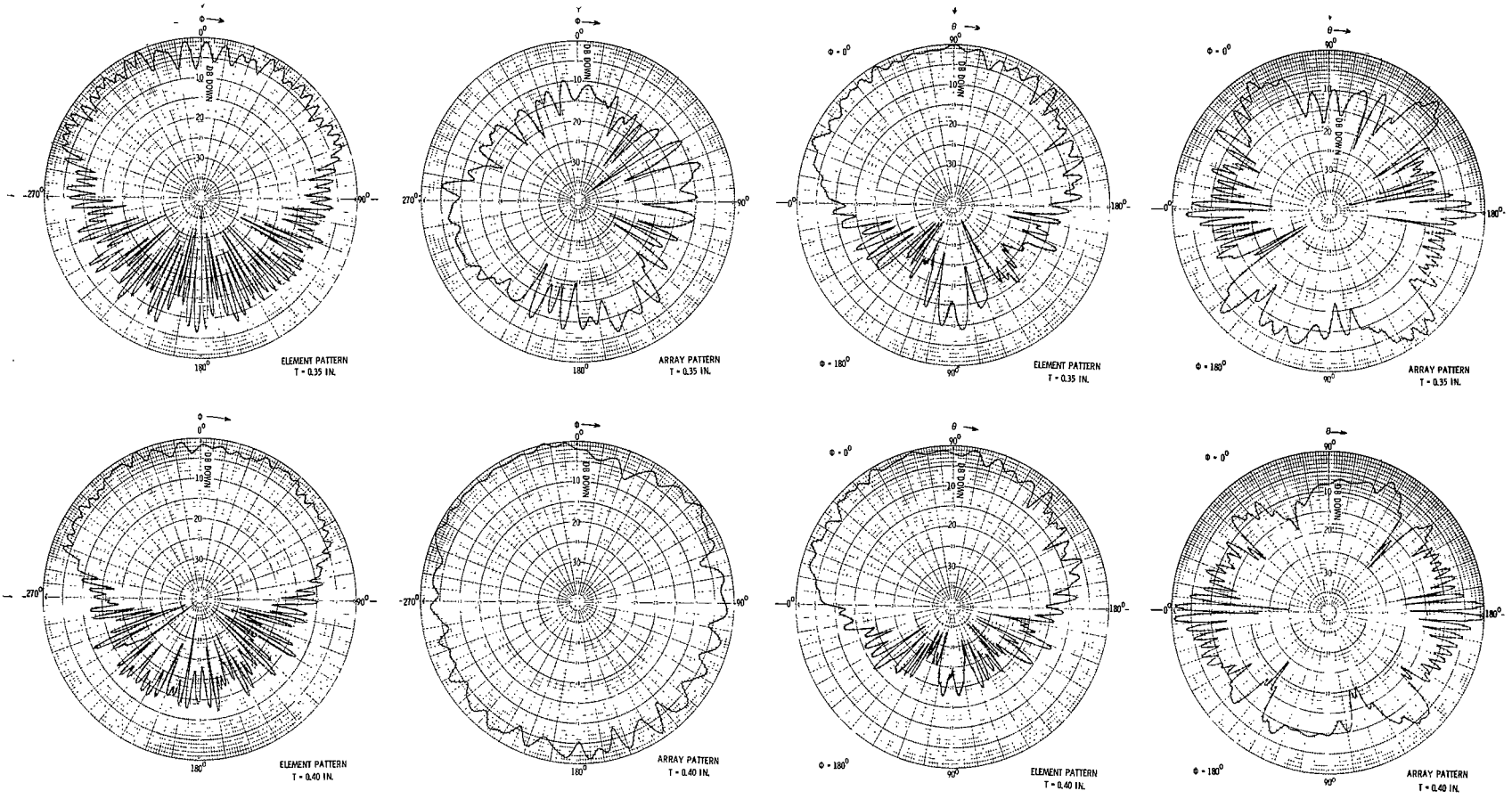
(a) $T = 0.00$ inch (0.00 cm) and $T = 0.20$ inch (0.51 cm).

Figure 9.- Measured elevation and azimuth and element and array patterns.



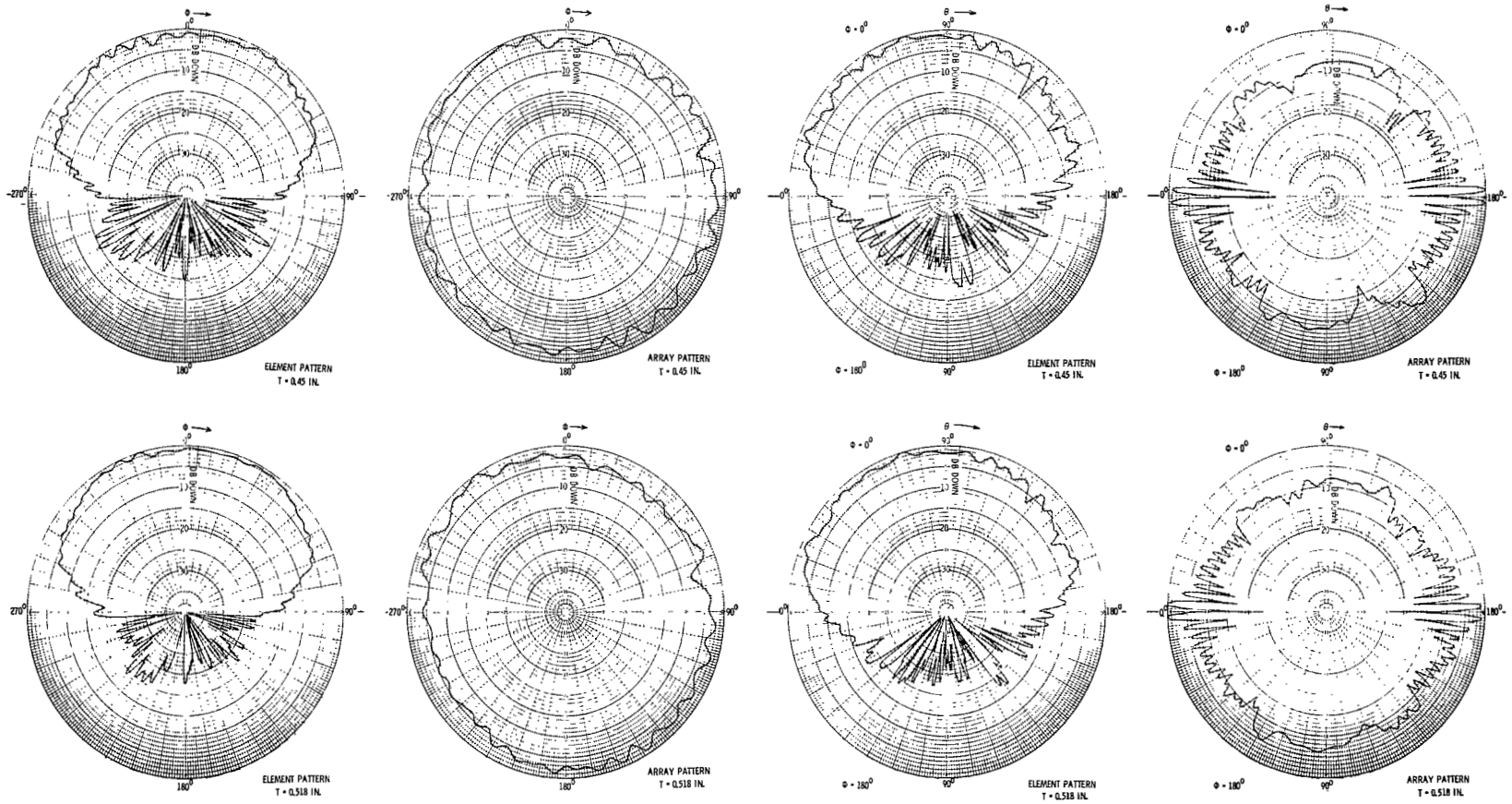
(b) $T = 0.25$ inch (0.645 cm) and $T = 0.30$ inch (0.76 cm).

Figure 9.- Continued.



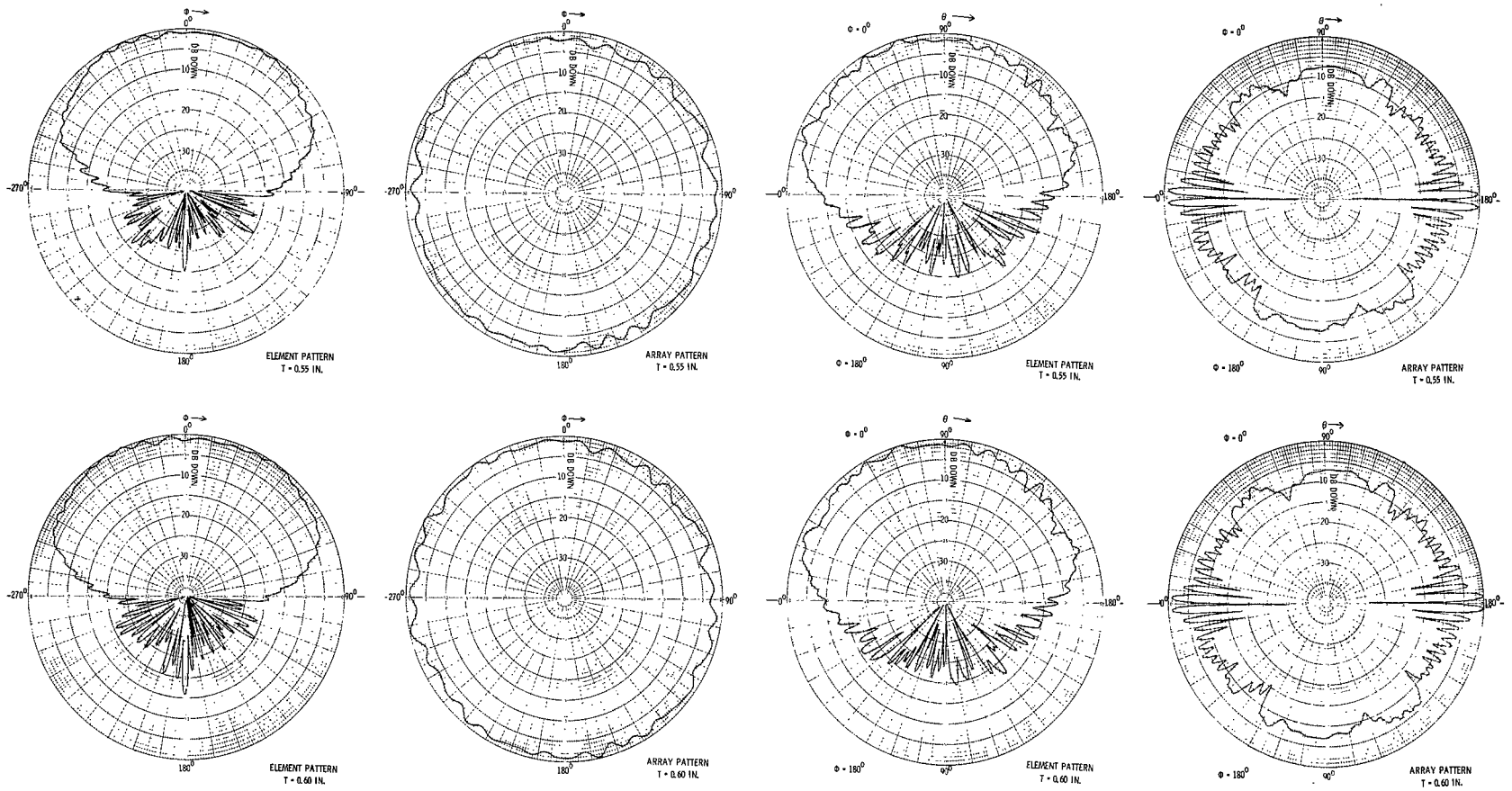
(c) $T = 0.35$ inch (0.89 cm) and $T = 0.40$ inch (1.016 cm).

Figure 9.- Continued.



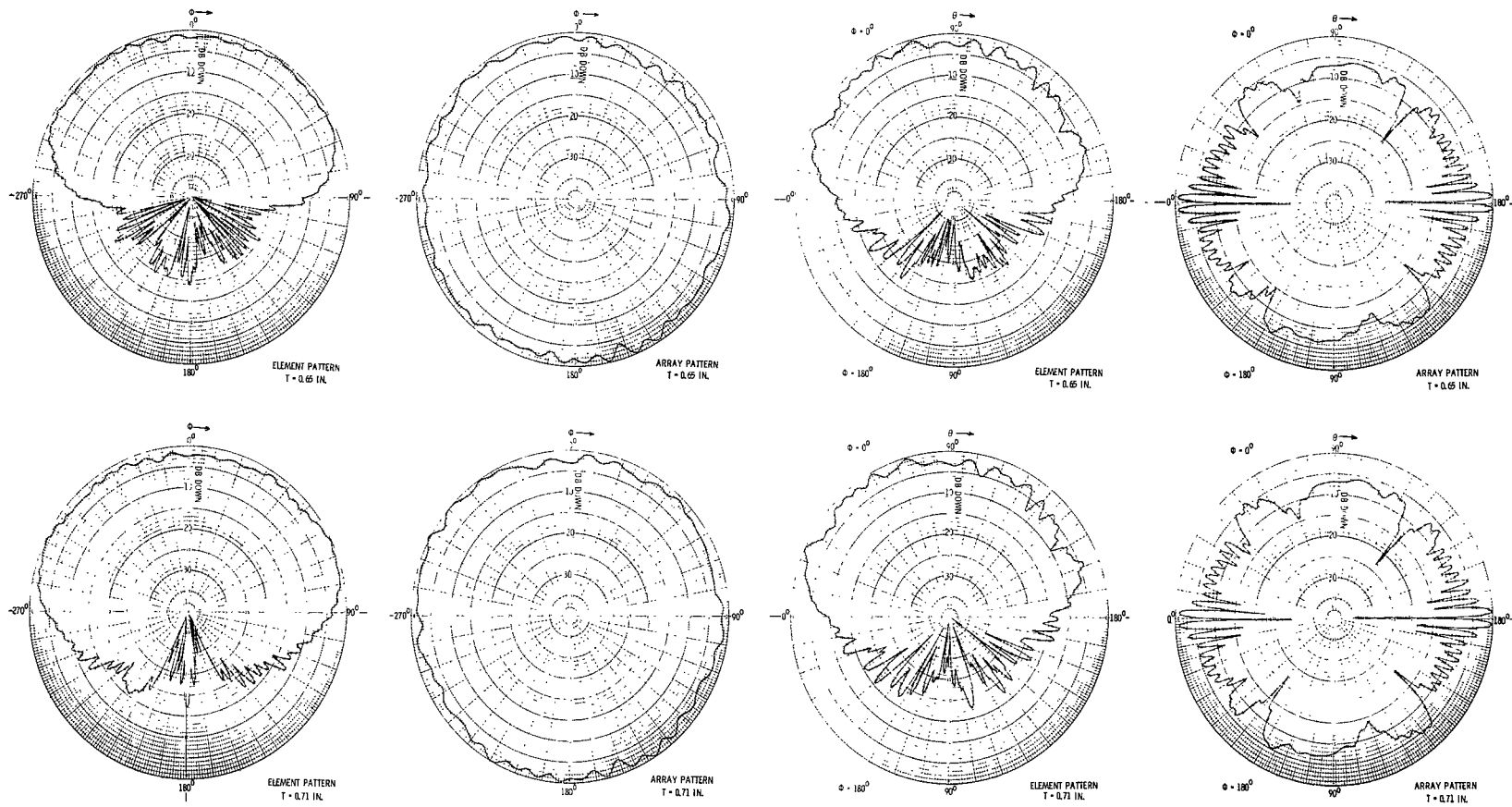
(d) $T = 0.45$ inch (1.14 cm) and $T = 0.518$ inch (1.316 cm).

Figure 9.- Continued.



(e) $T = 0.55$ inch (1.40 cm) and $T = 0.60$ inch (1.52 cm).

Figure 9.- Continued.



(f) $T = 0.65$ inch (1.65 cm) and $T = 0.71$ inch (1.80 cm).

Figure 9.- Concluded.

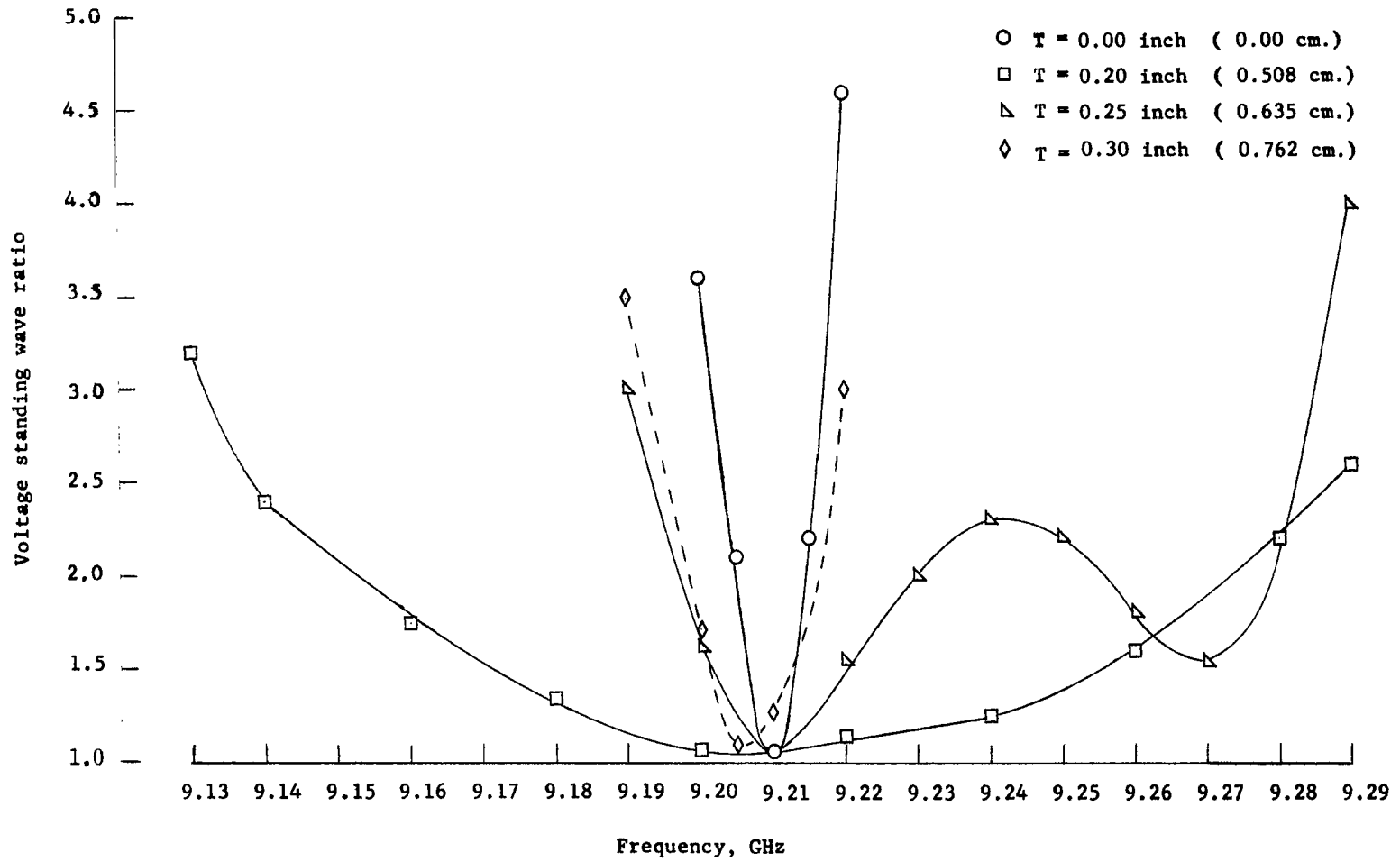


Figure 10.- Measured input voltage standing wave ratio of 54 slot array for various thicknesses of dielectric.

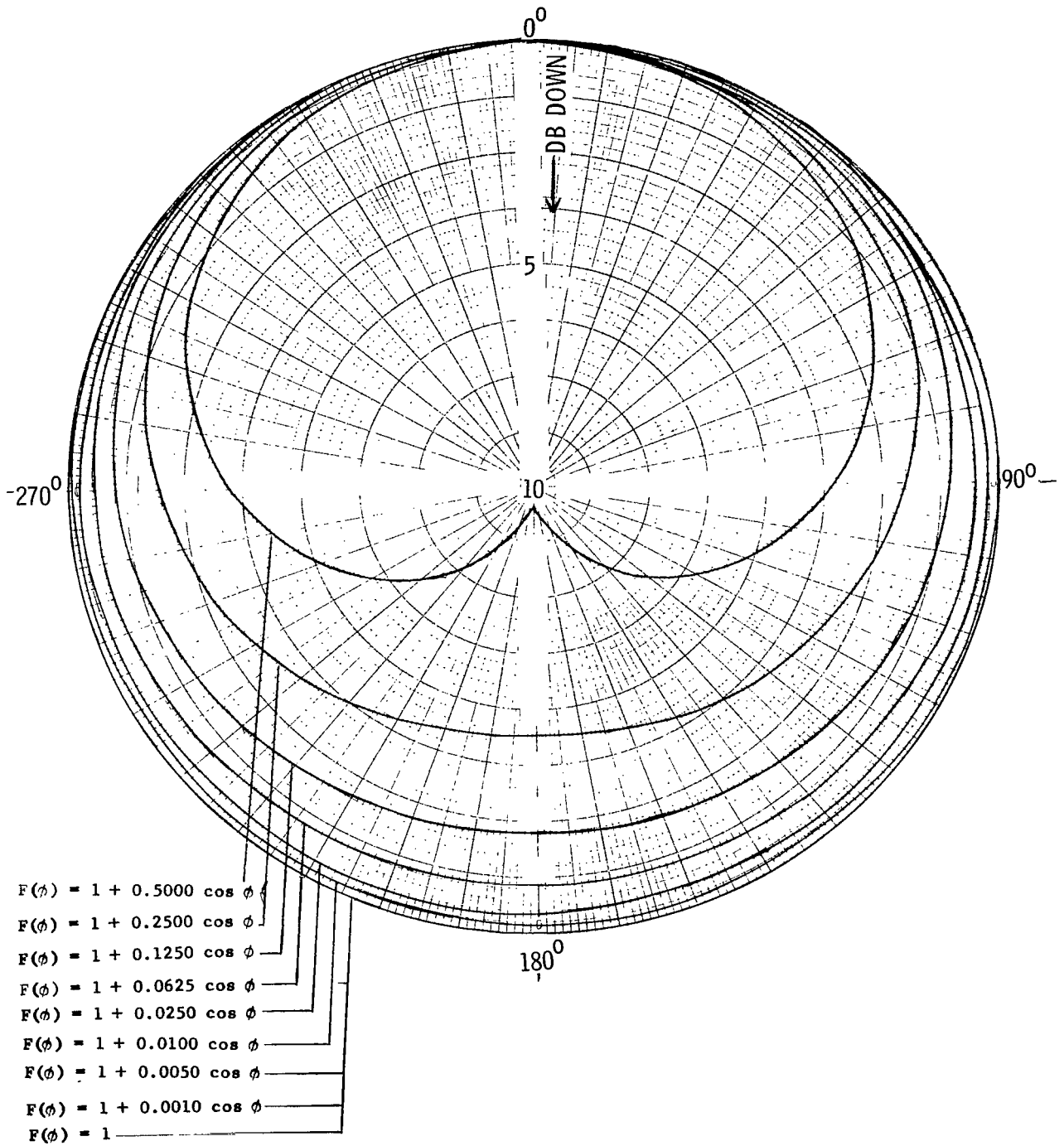


Figure 11.- Assumed element amplitude patterns. Normalized.

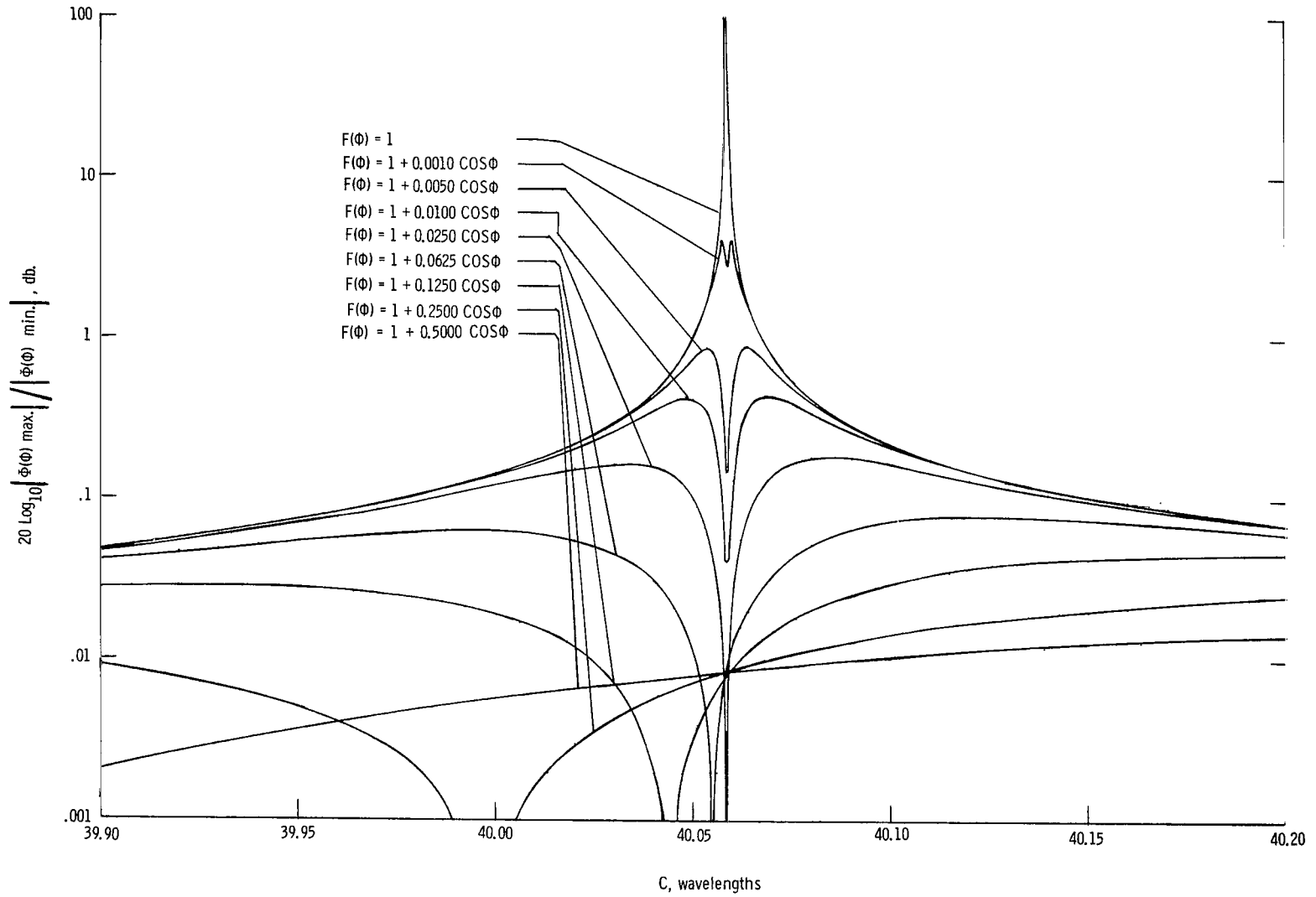


Figure 12.- Computed ripple D in array patterns for elements having various amplitude patterns.

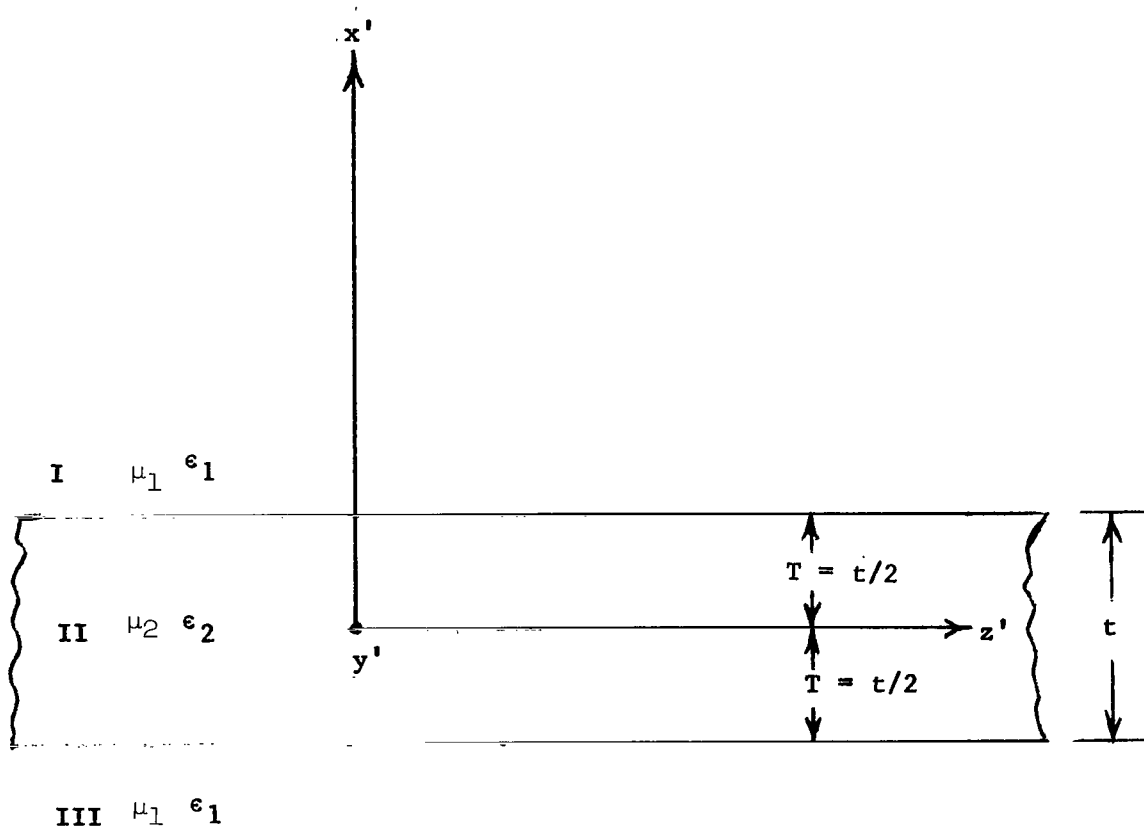
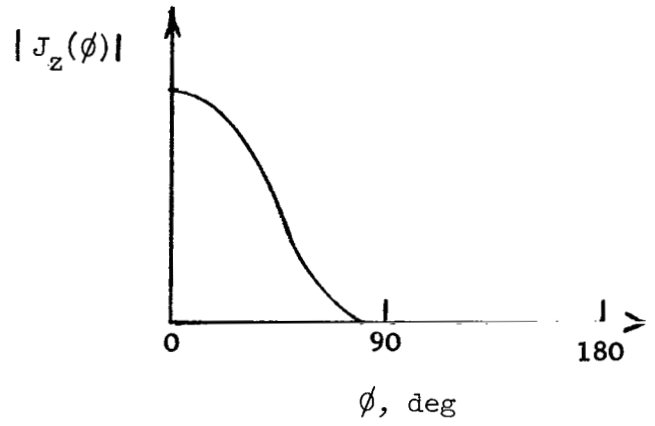
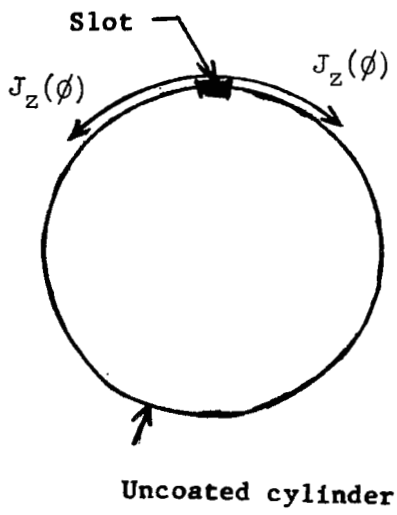
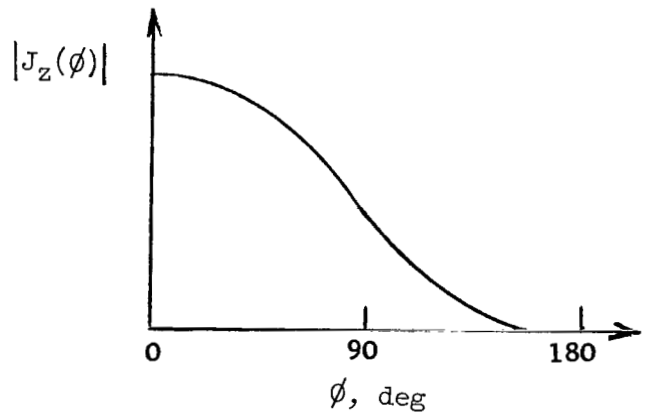
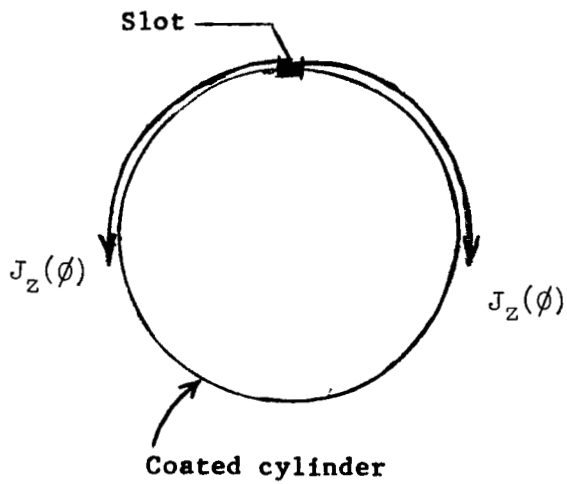


Figure 13.- Plane surface wave model.



(a) Uncoated case.



(b) Coated case.

Figure 14.- Current on cylinder excited by slot.

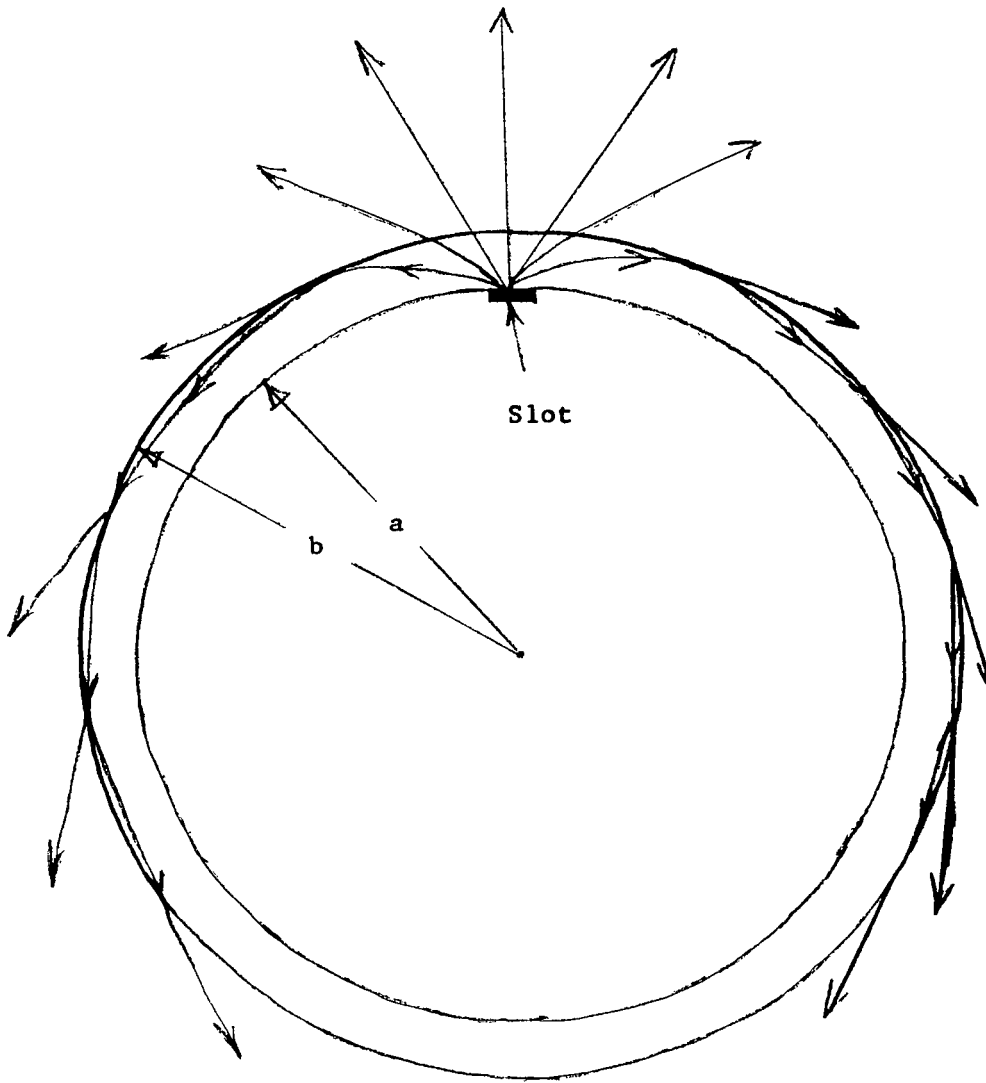


Figure 15.- Power flow diagram for coated cylinder.

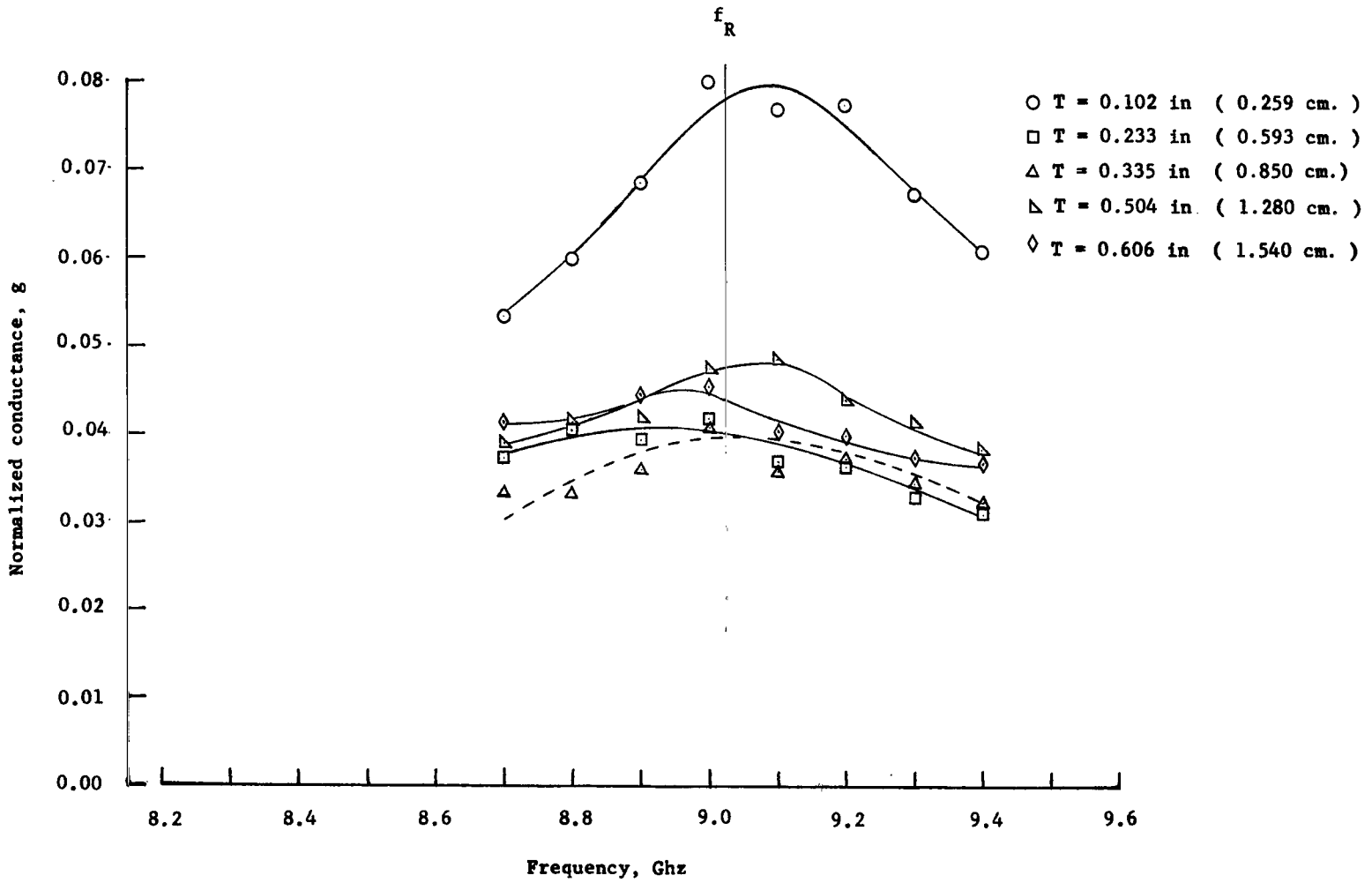


Figure 16.- Measured conductances of various thickness dielectric sheets ($\epsilon_r' = 2.54$).

OFFICIAL BUSINESS

14U 001 32 51 3DS 68059 00903
AIR FORCE WEAPONS LABORATORY/AFWL/
KIRTLAND AIR FORCE BASE, NEW MEXICO 87117

ATT MISS MADELINE F. CANOVA, CHIEF TECHNICAL
LIBRARY /WLIL/

POSTMASTER: If Undeliverable (Section 158
Postal Manual) Do Not Return

"The aeronautical and space activities of the United States shall be conducted so as to contribute . . . to the expansion of human knowledge of phenomena in the atmosphere and space. The Administration shall provide for the widest practicable and appropriate dissemination of information concerning its activities and the results thereof."

—NATIONAL AERONAUTICS AND SPACE ACT OF 1958

NASA SCIENTIFIC AND TECHNICAL PUBLICATIONS

TECHNICAL REPORTS: Scientific and technical information considered important, complete, and a lasting contribution to existing knowledge.

TECHNICAL NOTES: Information less broad in scope but nevertheless of importance as a contribution to existing knowledge.

TECHNICAL MEMORANDUMS: Information receiving limited distribution because of preliminary data, security classification, or other reasons.

CONTRACTOR REPORTS: Scientific and technical information generated under a NASA contract or grant and considered an important contribution to existing knowledge.

TECHNICAL TRANSLATIONS: Information published in a foreign language considered to merit NASA distribution in English.

SPECIAL PUBLICATIONS: Information derived from or of value to NASA activities. Publications include conference proceedings, monographs, data compilations, handbooks, sourcebooks, and special bibliographies.

TECHNOLOGY UTILIZATION PUBLICATIONS: Information on technology used by NASA that may be of particular interest in commercial and other non-aerospace applications. Publications include Tech Briefs, Technology Utilization Reports and Notes, and Technology Surveys.

Details on the availability of these publications may be obtained from:

SCIENTIFIC AND TECHNICAL INFORMATION DIVISION
NATIONAL AERONAUTICS AND SPACE ADMINISTRATION

Washington, D.C. 20546